J. Fluid Mech. (2010), *vol.* 651, *pp.* 357–385.
doi:10.1017/S002211200999406X

Linear instability of two-fluid Taylor–Couette flow in the presence of surfactant

JIE PENG† AND KE-QIN ZHU

Department of Engineering Mechanics, Tsinghua University, Beijing 100084, China

(Received 13 August 2009; revised 14 December 2009; accepted 15 December 2009; first published online 24 March 2010)

The effect of an insoluble surfactant on the centrifugal and shear instability of a pair of radially stratified immiscible liquids in the annular gap between concentric two-fluid Taylor–Couette flow is investigated by a normal-mode linear analysis and complementary energy analysis. The interface is assumed to be concentric with the cylinders. The gravitational effects are ignored. Influences of density and viscosity stratification, surface tension, surfactant concentration distribution and Taylor–Couette shearing are considered comprehensively. The instability characteristics due to competition and interaction between various physical instability mechanisms are of principal concern. Neutral curves with upper and lower branches in the Reynolds number (Re_1)/axial wavenumber (k) plane are obtained. A window of parameters is identified in which the flow is linearly stable. The Marangoni traction force caused by the gradient of surfactant concentration stabilizes the axisymmetric perturbations but initiates an instability corresponding to non-axisymmetric modes in the presence of basic Couette shearing flow. Co-rotation of the outer cylinder has a stabilizing effect in expanding the stable region, which dwindles in the counter-rotation situation.

1. Introduction

The swirling flow in the gap between two concentric cylinders, known as Taylor–Couette flow, has been extensively investigated for homogeneous fluids and gives a controlled access to different flow regimes, ranging from wavy flows and wavy-vortex flows to turbulence. The importance of the flow between coaxial cylinders as a fluid-dynamical paradigm has been well documented in the review by DiPrima & Swinney (1981). Although this flow has attracted many studies since the ground-breaking experimental and theoretical work of Taylor (1923), the extension to the flow of two fluids in the same geometry has received relatively little attention despite the potential for interesting interactions between centrifugal and interfacial instabilities. Furthermore, there are a number of interesting questions that arise from this hypothesis. From a purely fluid dynamical standpoint, the presence of the interface increases the range of potential flow patterns. On a more applied level, two-fluid Taylor–Couette flow may be of practical value for mass transfer operations through the liquid–liquid interface in the bioreactor/bioseparator. The possibility of such an enhancement has been demonstrated experimentally (Baier & Graham 1998; Baier, Graham & Lightfoot 2000) and theoretically (Baier & Graham 2000; Yarin, Gelfgat & Bar-Yoseph 2002).

† Email address for correspondence: peng-jie@tsinghua.edu.cn

The existence of this flow has been anticipated by Schneyer & Berger (1971) and Joseph, Nguyen & Beavers (1984). Schneyer & Berger (1971) reported a linear instability analysis of two incompressible, immiscible stratified fluids. The analysis assumed a stationary outer cylinder, negligible surface tension and gravitational effects. Joseph *et al.* (1985) studied the instability of rigid rotation of two centrifugally stratified fluids between coaxial cylinders while gravity was ignored. They found that the flow instability is determined by the dimensionless group

$$Q = (\rho_2^* - \rho_1^*)(\Omega^*)^2(R_s^*)^3/\gamma^*, \tag{1.1}$$

where ρ_1^* and ρ_2^* are the densities of the inner and outer fluid layers. Ω^* is the angular velocity of both cylinders, R_s^* is the radial position of the interface and γ^* is the surface tension. Linear and energy instability analysis predicts a linearly stable interface between the two fluids when $Q > 1$ and is globally stable when $Q > 4$. The Couette flow of two immiscible stratified fluids has been computationally explored by Renardy & Joseph (1985), assuming a stationary outer cylinder. The surface tension effects were considered. They pointed out that a thin layer of less viscous fluid next to either cylinder is linearly stable, and that it is possible to have stability with the less dense fluid lying outside when the centrifugal effect is overcome by an appropriate combination of surface tension. Reports of corresponding experimental works were also presented by Joseph and coworkers (Joseph & Renardy 1993) with a horizontal Couette cell. Recently, a three-dimensional computational fluid dynamics (CFD) numerical simulation of radially stratified, two-fluid Taylor–Couette flow was carried out by Vedantam, Joshi & Koganti (2006). To our knowledge, only a small number of studies have been performed on two-fluid Taylor–Couette flow with a stationary outer cylinder in the absence of an interfacial surfactant.

In general, the presence of even minute amounts of surfactant on a fluid–fluid interface can have a substantial effect on the evolution of the interface (Edwards, Brenner & Wasan (1991)). A number of authors have investigated the effect of an insoluble surfactant on the instability of a stationary arrangement. Carroll & Lucassen (1974) studied the formation of droplets from cylindrical oil films experimentally. Otis *et al.* (1993) numerically studied the role of surfactant in airway closure and the corresponding experimental results were presented by Cassidy *et al.* (1999). It has been pointed out that the surfactant may reduce the growth rate of interfacial perturbation. This is caused by the fact that surfactant can lower the surface tension and diminish the intensity of surface tension, thereby relieving interfacial distortion (Halpern & Grotberg 1993; Blyth & Pozrikidis 2004*a*). However, Frenkel & Halpern (2002), Halpern & Frenkel (2003) and Blyth & Pozrikidis (2004*b*) recently discovered that the presence of an insoluble surfactant on a two-dimensional planar sheared interface induces a Marangoni instability, even with the assumption of Stokes flow. A Marangoni traction force is induced due to the presence of surfactant concentration gradient along the interface, which can influence the system instability through its interaction with the basic shearing flow. The role of the basic shearing flow in affecting the instability of a surfactant-laden system lies in the interfacial tangential stress condition and the surfactant transport equation. The former gives rise to a jump in the shear stress across the interface, which can induce a flow instability. The latter is primarily due to surface convection, which can rearrange the surfactant distribution along the interface (Wei 2005, Wei & Rumschitzki 2005). Blyth, Luo & Pozrikidis (2006) investigated the effect of an insoluble surfactant on the instability of a core-annular flow of two immiscible fluids by a nonlinear calculation and

normal-mode linear analysis with only considering the axisymmetric perturbation. The results revealed that though the Marangoni traction force due to surfactant concentration gradient was unable to initiate a new type of instability, as in the case of two-dimensional two-layer channel flow, it destabilized the interface by broadening the range of growing wavenumbers and by raising the growth rate of unstable perturbations. As far as we know, the instability of a two-layer Taylor–Couette flow in the presence of a surfactant on the interface has not been studied before.

In the present work, we investigate the instability of two immiscible fluids with different density and viscosity separated by an interface with an insoluble surfactant and contained between two concentric cylinders that can rotate independently. Thus, in this system, the flow instabilities contain the following: (i) the Rayleigh–Taylor instability due to density difference (Sharp 1984; Kull 1991); (ii) the Yih instability inspired by an interfacial jump in viscosity (Yih 1967; Joseph & Renardy 1993; Charru & Hinch 2000); (iii) the Rayleigh–Tomotika capillary instability, which is driven by the surface tension (Newhouse & Pozrikidis 1992); (iv) the Marangoni instability, which is generated by surfactant convection and diffusion along the interface; and (v) the Taylor–Couette instability, if the inner cylinder rotates above a critical speed. In order to investigate the interaction of the above instability mechanisms in more detail, a normal-mode linear stability analysis was adopted while performing a complementary energy analysis. The instabilities for both axisymmetric and non-axisymmetric perturbations were investigated comprehensively. We found that there is an interval of Reynolds number within which the flow is stable for perturbations with all axial wavenumbers. Our analysis goes beyond that given by Renardy & Joseph (1985) and Baier & Graham (1998, 2000), because the effects of surface tension, viscosity and density stratifications, surfactant concentration and rotation of inner and outer cylinders are all considered.

The content of the paper is as follows. A complete physical and numerical description of the problem is given in § 2. The linear differential equations about the linear instability for the small perturbations are obtained by using normal modes. The energy analysis is also given as a complement. In § 3, the numerical implementation of this eigenvalue problem is presented together with corresponding verification. The main results are given in § 4, where the interactions between the above instability mechanisms are presented. In § 5, the conclusions are presented.

2. Problem formulation

In this paper, we consider the Taylor–Couette flow of two immiscible Newtonian fluids between two concentric rotating cylinders, whose radii and angular velocities are R_1^*, R_2^* and Ω_1^*, Ω_2^* see figure 1). The inner fluid is referred to as fluid 1 with density ρ_1^* and dynamic viscosity μ_1^*, whereas the outer fluid is denoted fluid 2 with density and dynamic viscosity ρ_2^* and μ_2^*.

The interface is occupied by an insoluble surfactant, which can convect and diffuse along the interface to alter the local surface tension. The unperturbed, insoluble surfactant concentration Γ_0^* is assumed to be uniform over the interface, with corresponding surface tension γ_0^*. Without loss of generality, the equation of γ^* can be expanded in Taylor series around the unperturbed basic state. Because the linear problem is considered in this paper, the first-order expression of the series is

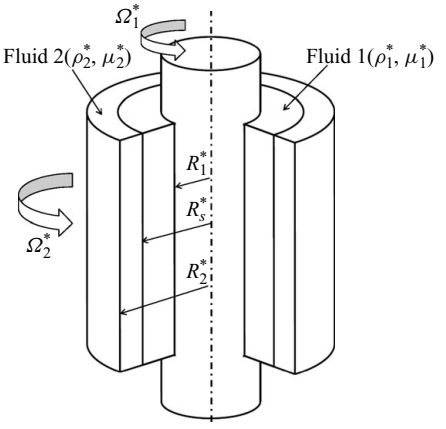

FIGURE 1. Geometric sketch and parameters of the two-fluid Taylor–Couette flow.

retained, with additional terms being truncated as

$$\gamma^* = \gamma_0^* - \beta(\Gamma^* - \Gamma_0^*) + O(\Gamma^* - \Gamma_0^*)^2 \approx \gamma_0^* - \beta(\Gamma^* - \Gamma_0^*), \tag{2.1}$$

where $\beta = -(\partial\gamma^*/\partial\Gamma^*)_{\Gamma_0^*}$. In this paper, following Halpern & Frenkel (2003), we can obtain the convection–diffusion equation of surfactant concentration Γ^* in cylindrical coordinates (Appendix A), which can also be derived from the one given by Li & Pozrikidis (1997).

$$\frac{\partial}{\partial t}(\Gamma^* S^* H) + \frac{\partial}{\partial\theta}(u_\theta^* \Gamma^* H) + \frac{\partial}{\partial z}(u_z^* S^* \Gamma^* H) = D_s^* \frac{\partial}{\partial\theta}\left(\frac{H}{\sqrt{1+\left(\dfrac{\partial S^*}{S^*\partial\theta}\right)^2}}\frac{\partial\Gamma^*}{S^*\partial\theta}\right) + D_s^* \frac{\partial}{\partial z}\left(\frac{HS^*}{\sqrt{1+\left(\dfrac{\partial S^*}{\partial z}\right)^2}}\frac{\partial\Gamma^*}{\partial z}\right), \tag{2.2}$$

where

$$H = \sqrt{1+\left(\frac{\partial S^*}{S^*\partial\theta}\right)^2 + \left(\frac{\partial S^*}{\partial z}\right)^2}. \tag{2.3}$$

D_s^* is the surface molecular diffusivity of surfactant. $S^*(\theta, z)$ is the local radius of the interface. We introduce dimensionless variables as

$$\varepsilon = \frac{R_s^*}{R_2^*},\ \ \eta = \frac{R_1^*}{R_2^*},\ \ \alpha = \frac{\mu_1^*}{\mu_2^*},\ \ \delta = \frac{\rho_1^*}{\rho_2^*},\ \ \gamma = \frac{\gamma^*}{\gamma_0^*},\ \ \Gamma = \frac{\Gamma^*}{\Gamma_0^*},\ \ S = \frac{S^*}{R_2^*}, \tag{2.4}$$

where R_2^*, $\rho_2^* R_2^{*2}/\mu_2^*$ and $(\mu_2^*)^2/\rho_2^* R_2^{*2}$ are adopted as units for space, time, pressure or stress. R_s^* indicates the radius of initial unperturbed interface. Hereinafter, all variables will be rendered dimensionless with the above units. The dimensionless form of (2.1) is

$$\gamma = 1 - M(\Gamma - 1). \tag{2.5}$$

Here, $M = \beta\Gamma_0^*/\gamma_0^*$ is defined as a dimensionless Marangoni number. The rotation speeds of inner and outer cylinders are described by the rotation Reynolds numbers $Re_1 = \rho_2^* R_1^* R_2^* \Omega_1^*/\mu_2^*$ and $Re_2 = \rho_2^* \Omega_2^* R_2^{*2}/\mu_2^*$, independently.

2.1. *Governing equation and basic shearing flow*

The dimensionless continuity and momentum equations in vector form are

$$\nabla \cdot \boldsymbol{u}_q = 0, \tag{2.6}$$

$$\delta_q(\partial_t \boldsymbol{u}_q + \boldsymbol{u}_q \cdot \nabla \boldsymbol{u}_q) = -\nabla p_q + \nabla \cdot \boldsymbol{\tau}_q, \tag{2.7}$$

where $q = 1, 2$ denotes the stratified fluid regions with $\delta_1 = \delta$ and $\delta_2 = 1$. The cylindrical coordinate system is adopted with the radial, azimuthal and axial directions being denoted by r, θ and z, respectively. Here, $\boldsymbol{u}_q = (u_r, u_\theta, u_z)_q$ denotes the flow velocity and $\boldsymbol{\tau}_q = \alpha_q \left(\nabla \boldsymbol{u}_q + \nabla \boldsymbol{u}_q{}^{\mathrm{T}}\right)$ is the tensor of viscous shearing stress with $\alpha_1 = \alpha$ and $\alpha_2 = 1$. The boundary condition on the cylinder wall is defined as

$$\boldsymbol{u}_q = \left(0, Re_q, 0\right), \quad at \quad r = \eta, 1. \tag{2.8}$$

In the absence of perturbation, the piecewise azimuthal Couette shearing velocity profile of the basic shearing flow is given by

$$\overline{u}_{\theta 1} = A_1 r + \frac{B_1}{r}, \quad \text{for} \quad \eta < r < \varepsilon, \tag{2.9a}$$

$$\overline{u}_{\theta 2} = A_2 r + \frac{B_2}{r}, \quad \text{for} \quad \varepsilon < r < 1. \tag{2.9b}$$

According to the boundary condition (2.8) and continuous conditions of velocities and shearing stresses across the interface, the constants can be determined as

$$A_1 = \frac{(\alpha-1)Re_1\eta + (Re_2 - \alpha\eta Re_1)\varepsilon^2}{(\varepsilon^2-\eta^2) + \alpha\eta^2(1-\varepsilon^2)}, \quad B_1 = \frac{(Re_1 - Re_2\eta)\eta\varepsilon^2}{(\varepsilon^2-\eta^2) + \alpha\eta^2(1-\varepsilon^2)}, \tag{2.10a}$$

$$A_2 = \frac{(\alpha-1)Re_2\eta^2 + (Re_2 - \alpha\eta Re_1)\varepsilon^2}{(\varepsilon^2-\eta^2) + \alpha\eta^2(1-\varepsilon^2)}, \quad B_2 = \frac{\alpha(Re_1 - Re_2\eta)\eta\varepsilon^2}{(\varepsilon^2-\eta^2) + \alpha\eta^2(1-\varepsilon^2)}. \tag{2.10b}$$

2.2. *Formulation of the linear stability problem*

Considering an infinitesimal perturbation to the basic shearing flow, in the normal-mode analysis, it is assumed to be periodic in the axial and azimuthal directions, with n and k denoting the respective real wavenumbers

$$\begin{pmatrix} v_r \\ v_\theta \\ v_z \\ p \end{pmatrix}_q (r, \theta, z, t) = \begin{pmatrix} 0 \\ \overline{u}_\theta(r) \\ 0 \\ \overline{p}(r) \end{pmatrix}_q + \begin{pmatrix} V_r(r) \\ V_\theta(r) \\ V_z(r) \\ P(r) \end{pmatrix}_q \mathrm{e}^{\mathrm{i}(n\theta + kz + ct)}. \tag{2.11}$$

For each fluid q, the linearized governing equations (2.6) and (2.7) around the basic shearing flow yield

$$\left(\mathrm{D}V_r + \frac{\mathrm{i}n}{r}V_\theta + \mathrm{i}kV_z + \frac{V_r}{r}\right)_q = 0, \tag{2.12}$$

$$\left[\mathrm{i}\left(c + n\frac{\overline{u}_\theta}{r}\right)V_r - \frac{2\overline{u}_\theta}{r}V_\theta\right]_q = -\frac{1}{\delta_q}\mathrm{D}P_q + \frac{\alpha_q}{\delta_q} \times \left(\mathrm{D}^2 V_r + \frac{1}{r}\mathrm{D}V_r - \frac{n^2}{r^2}V_r - k^2 V_r - \frac{\mathrm{i}2n}{r^2}V_\theta - \frac{V_r}{r^2}\right)_q, \tag{2.13}$$

$$\left[\mathrm{i}\left(c+n\frac{\overline{u}_\theta}{r}\right)V_\theta+V_r\mathrm{D}\overline{u}_\theta+\frac{\overline{u}_\theta}{r}V_r\right]_q=-\frac{\mathrm{i}n}{\delta_q r}P_q + \frac{\alpha_q}{\delta_q}\left(\mathrm{D}^2V_\theta+\frac{1}{r}\mathrm{D}V_\theta-\frac{n^2}{r^2}V_\theta-k^2V_\theta+\frac{2\mathrm{i}n}{r^2}V_r-\frac{V_\theta}{r^2}\right)_q, \quad (2.14)$$

$$\left[\mathrm{i}\left(c+n\frac{\overline{u}_\theta}{r}\right)V_z\right]_q=-\frac{1}{\delta_q}\mathrm{i}kP_q+\frac{\alpha_q}{\delta_q}\left(\mathrm{D}^2V_z+\frac{1}{r}\mathrm{D}V_z-\frac{n^2}{r^2}V_z-k^2V_z\right)_q. \quad (2.15)$$

Here, $\mathrm{D}=\partial/\partial r$. The interface is also assumed to displace to a new position with infinitesimal perturbation around the initial unperturbed position. The dimensionless interface radius $S(\theta,z)$ is then described by

$$S(\theta,z)=\varepsilon+X\mathrm{e}^{\mathrm{i}(n\theta+kz+ct)}. \quad (2.16)$$

The surfactant distribution with corresponding perturbation to the uniform surfactant concentration is expressed as

$$\Gamma(\theta,z)=1+\Psi\mathrm{e}^{\mathrm{i}(n\theta+kz+ct)}. \quad (2.17)$$

Linearizing the kinematic condition at the interface ($r=\varepsilon$), we have

$$\mathrm{i}cX-V_r+\mathrm{i}n\frac{\overline{u}_\theta}{\varepsilon}X=0. \quad (2.18)$$

The linearized form of the surfactant convection–diffusion equation (2.2) is written as

$$\mathrm{i}\frac{V_r}{\varepsilon}-\frac{n}{\varepsilon}V_\theta-kV_z+\left[\mathrm{i}D_s\left(\frac{n^2}{\varepsilon^2}+k^2\right)-\left(c+\frac{n}{\varepsilon}\overline{u}_\theta\right)\right]\Psi=n\left(\frac{\mathrm{D}\overline{u}_\theta}{\varepsilon}-\frac{\overline{u}_\theta}{\varepsilon^2}\right)X, \quad (2.19)$$

where $D_s=D_s^*\rho_2^*/\mu_2^*$ is the dimensionless interfacial diffusivity of the surfactant. The following linearized conditions hold at the interface $r=\varepsilon$, which can be written as

(i) Continuity of velocity:

$$[\![V_r]\!]=0,\quad [\![V_\theta]\!]+[\![\mathrm{D}\overline{u}_\theta]\!]X=0,\quad [\![V_z]\!]=0. \quad (2.20)$$

(ii) Balance of normal and tangential stresses along r, θ, and z directions:

$$[\![2\alpha\mathrm{D}V_r-P]\!]-\left[\!\!\left[\delta\frac{\overline{u}_\theta{}^2}{\varepsilon}\right]\!\!\right]X+J\left[\frac{M}{\varepsilon}\Psi+\frac{X}{\varepsilon^2}-\left(\frac{n^2}{\varepsilon^2}+k^2\right)X\right]=0, \quad (2.21a)$$

$$[\![\alpha\mathrm{D}V_\theta]\!]+\frac{\mathrm{i}n}{\varepsilon}[\![\alpha V_r]\!]-\frac{1}{\varepsilon}[\![\alpha V_\theta]\!]-\frac{\mathrm{i}n}{\varepsilon}JM\Psi=0, \quad (2.21b)$$

$$[\![\alpha\mathrm{D}V_z]\!]+\mathrm{i}k[\![\alpha V_r]\!]-\mathrm{i}kJM\Psi=0. \quad (2.21c)$$

Here, we define the jump notation $[\![\cdot]\!]=(\cdot)_2-(\cdot)_1$. Derivation of (2.21$a$)–(2.21$c$) is described in detail in Appendix B. J is the dimensionless surface tension parameter with definition

$$J=\frac{\rho_2^*\gamma_0^*R_2^*}{(\mu_2^*)^2}. \quad (2.22)$$

Apparently, J is independent of the flow characteristics. We require all the perturbation velocities to vanish at the cylinder walls. Thus, the boundary conditions of perturbation velocities are

$$V_r=V_\theta=V_z=0,\quad at\ \ r=\eta,1. \quad (2.23)$$

From the above equations, we know that the system instability is characterized by the following nine dimensionless parameters

$$Re_1,\ Re_2,\ \eta,\ \varepsilon,\ \alpha,\ \delta,\ J,\ M,\ D_s. \tag{2.24}$$

Here, Re_1, Re_2 indicate the rotation speeds of inner and outer cylinders. η denotes the ratio of cylinder radius. ε denotes the dimensionless interface position. α and δ indicate the viscosity and density ratios of the stratified fluids. J denotes the dimensionless surface tension, M is the Marangoni number and D_s indicates the dimensionless surfactant interfacial diffusivity.

2.3. *Energy analysis*

The linear instability of the flow can be determined by the equations listed in the above section. However, they do not provide information regarding the mechanism driving the instability. From § 1, we know that the flow characteristics are dominated by five instability mechanisms. In order to figure out the situations in which instability is introduced by the surface tension or Reynolds stress, the perturbation energy (Hu & Joseph 1989) is evaluated. After multiplying (2.13), (2.14) and (2.15) with the complex conjugates of perturbation velocities, respectively, they are integrated over the flow regions Ω_q ($q = 1, 2$ indicate the flow regions $\Omega_1 = [\eta, \varepsilon]$ and $\Omega_2 = [\varepsilon, 1]$) and added together. Combining with (2.12) and (2.23), we can obtain

$$\begin{aligned}
&\mathrm{i}c\sum_{q=1}^{2}\int_{\Omega_q}\delta_q\left(|V_r|^2+|V_\theta|^2+|V_z|^2\right)_q r\,\mathrm{d}r+\mathrm{i}\sum_{q=1}^{2}\int_{\Omega_q}\delta_q n\left[\overline{u}_\theta\left(|V_r|^2+|V_\theta|^2+|V_z|^2\right)\right]_q\mathrm{d}r\\
&\quad=\sum_{q=1}^{2}\int_{\Omega_q}\delta_q\left[2\frac{\overline{u}_\theta}{r}V_\theta\widetilde{V}_r-\left(\mathrm{D}\overline{u}_\theta+\frac{\overline{u}_\theta}{r}\right)V_r\widetilde{V_\theta}\right]_q r\,\mathrm{d}r\\
&\qquad-\sum_{q=1}^{2}\int_{\Omega_q}\alpha_q\left[2\left(|V_r|^2+\left|\frac{\mathrm{i}nV_\theta+V_r}{r}\right|^2+|kV_z|^2\right)+\left|\mathrm{D}V_\theta+\frac{\mathrm{i}nV_r-V_\theta}{r}\right|^2\right.\\
&\qquad\left.+\left|\frac{\mathrm{i}nV_z}{r}+\mathrm{i}kV_\theta\right|^2+|\mathrm{D}V_z+\mathrm{i}kV_r|^2\right]_q r\,\mathrm{d}r\\
&-[\![-\widetilde{V_r}\,P+2\alpha\widetilde{V_r}\,DV_r+\alpha\widetilde{V_\theta}\mathrm{D}V_\theta+\alpha\frac{\mathrm{i}n}{r}\widetilde{V_\theta}V_r-\alpha\frac{\widetilde{V_\theta}V_\theta}{r}+\alpha\mathrm{i}k\widetilde{V_z}\,V_r+\alpha\widetilde{V_z}\,\mathrm{D}V_z]\!]_{r=\varepsilon},
\end{aligned}\tag{2.25}$$

Here, ' $\sim$ ' denotes the complex conjugate and $|V_r|^2=\widetilde{V_r}\,V_r$, $|V_\theta|^2=\widetilde{V_\theta}V_\theta,\ldots$. Each term in (2.25) is some kind of energy; thus, it represents the energy balance for the flow perturbation. The real part of (2.25) governs the energy growth rate of small perturbations, and it can be separated into the following four terms

$$\dot{E}=\Theta-\Phi+I, \tag{2.26}$$

where

$$\dot{E}=\lambda\sum_{q=1}^{2}\int_{\Omega_q}\delta_q\left(|V_r|^2+|V_\theta|^2+|V_z|^2\right)_q r\,\mathrm{d}r, \tag{2.27}$$

$$\Theta = \sum_{q=1}^{2} \mathrm{Re}\left\{ \int_{\Omega_q} \delta_q \left[2\frac{\overline{u}_\theta}{r} V_\theta \widetilde{V_r} - \left(\mathrm{D}\overline{u}_\theta + \frac{\overline{u}_\theta}{r} \right) V_r \widetilde{V_\theta} \right]_q r\,\mathrm{d}r \right\}, \tag{2.28}$$

$$\Phi = \sum_{q=1}^{2} \int_{\Omega_q} \alpha_q \left[2\left(|\mathrm{D}V_r|^2 + \left| \frac{\mathrm{i}nV_\theta + V_r}{r} \right|^2 + |kV_z|^2 \right) + \left| \mathrm{D}V_\theta + \frac{\mathrm{i}nV_r - V_\theta}{r} \right|^2 + \left| \frac{\mathrm{i}nV_z}{r} + \mathrm{i}kV_\theta \right|^2 + |\mathrm{D}V_z + \mathrm{i}kV_r|^2 \right]_q r\,\mathrm{d}r. \tag{2.29}$$

Here, $\lambda = -\mathrm{Im}(c)$ is the growth rate of perturbation, $\dot{E}$ is the rate of change of kinetic energy of the perturbed flow, Θ is the rate at which energy is transferred from the parallel basic shearing flow to the perturbed flow through Reynolds stress, Φ is the rate of viscous dissipation and I is the rate at which energy is supplied at the interface. Combining linearized equations (2.18)–(2.20) and (2.21*a*)–(2.21*c*) held at the interface $r = \varepsilon$ with surfactant diffusivity D_s being ignored, I can be written as

$$I = I_1 + I_2 + I_3 + I_4 + I_5, \tag{2.30}$$

where

$$I_1 = \lambda \frac{|V_r|^2}{|C|^2} (\delta - 1)\, \overline{u}_\theta^2, \tag{2.31}$$

$$I_2 = \lambda\varepsilon \frac{|V_r|^2}{|C|^2} \left(\frac{1 - n^2}{\varepsilon^2} - k^2 \right) J, \tag{2.32}$$

$$I_3 = n\frac{JM}{|C|^4} \left(\frac{\mathrm{D}\overline{u}_\theta}{\varepsilon} - \frac{\overline{u}_\theta}{\varepsilon^2} \right) \mathrm{Re}\left[\left(\mathrm{i}\,|V_r|^2 + n\widetilde{V_\theta} V_r + k\varepsilon \widetilde{V_z}\, V_r \right) \widetilde{C}\, \widetilde{C} \right] - \frac{JM}{\varepsilon\,|C|^2} |(V_r + \mathrm{i}nV_\theta + \mathrm{i}k\varepsilon V_z)|^2\, \lambda, \tag{2.33}$$

$$I_4 = -\frac{(\alpha - 1)}{\alpha\,|C|^2} \left(\mathrm{D}\overline{u}_\theta - \frac{\overline{u}_\theta}{\varepsilon} \right) \left[\mathrm{Re}\left(nC\,|V_r|^2 \right) + \mathrm{Im}\left(\varepsilon C \widetilde{V_r}\, \mathrm{D}V_\theta - C\widetilde{V_r}\, V_\theta \right) \right], \tag{2.34}$$

$$I_5 = -n\frac{(\alpha - 1)}{\alpha\,|C|^2} JM \left(\mathrm{D}\overline{u}_\theta - \frac{\overline{u}_\theta}{\varepsilon} \right) \mathrm{Re}\left(\frac{n}{\varepsilon} \widetilde{V_r}\, V_\theta + k\widetilde{V_r}\, V_z \right) - n^2 \frac{(\alpha - 1)\,|V_r|^2}{\varepsilon\alpha\,|C|^4} JM \left(\mathrm{D}\overline{u}_\theta - \frac{\overline{u}_\theta}{\varepsilon} \right)^2 \lambda. \tag{2.35}$$

Here, $C = c + n\overline{u}_\theta/\varepsilon$ and all the perturbation velocities are defined at the interface $r = \varepsilon$ in the flow region Ω_2. Note that I_1 represents the energy supplied at the interface due to the density stratification. If $I_1 < 0$, the flow is stabilized for $\delta < 1$, which means the flow is more stable with the denser fluid coating the outer cylinder. In addition, I_2 gives the energy supplied due to surface tension. Similar to Hu & Joseph (1989) and Kwak & Pozrikidis (2001), the surface tension destabilizes ($I_2 > 0$) long axisymmetric ($n = 0, k < 1/\varepsilon$) perturbation waves and stabilizes ($I_2 < 0$) short ($k > 1/\varepsilon$) or non-axisymmetric ($n \neq 0$) perturbation waves. Furthermore, I_3 denotes the energy supplied due to the effects of the surfactant. In the absence of basic

shearing flow ($\overline{u}_\theta = 0$), $I_3 < 0$, which indicates that the effect of surface tension can be slowed down due to the existence of surfactant. In the presence of basic shearing flow, the consequence of using surfactant is the development of surfactant concentration gradient and accompanying Marangoni traction force, which can also supply energy to perturbed flow. For $n = 0$, the first term of I_3 equals 0. This indicates that the basic shearing flow has few effects on the axisymmetric ($n = 0$) mode induced by Marangoni traction force. Moreover, I_4, which is proportional to the shearing strain of basic shearing flow, is the energy supplied due to viscosity jump across the interface and I_5, which is zero for $n = 0$, represents the energy supplied due to the coupling effect of Marangoni traction force and interfacial friction induced by viscosity stratification.

3. Numerical implementation

We employ a spectral collocation method based on Chebyshev polynomials to discretize the perturbation equations (2.12)–(2.23). Each of the two fluid regions, $\Omega_1 = [\eta, \varepsilon]$ and $\Omega_2 = [\varepsilon, 1]$, is mapped onto the standard interval $-1 \leqslant x_q \leqslant 1$ ($q = 1, 2$) using the following linear transformation:

$$x_1 = \frac{2r - \varepsilon - \eta}{\varepsilon - \eta} \text{ for } \Omega_1, \quad x_2 = \frac{2r - \varepsilon - 1}{1 - \varepsilon} \text{ for } \Omega_2. \tag{3.1}$$

In order to cluster the grid points near the interface, the Gauss–Lobatto points are adopted (Govindarajan 2004). In the non-staggered collocation method, artificial boundary conditions for the pressure at cylinder walls are needed. It is normally derived from the radial momentum equation (2.13), evaluated at the boundary walls, as

$$\mathrm{D}P = \alpha \mathrm{D}^2 V_r \ \ at \ \ r = \eta, \quad \mathrm{D}P = \mathrm{D}^2 V_r \ \ at \ \ r = 1. \tag{3.2}$$

Khorrami (1991) has shown that a non-staggered grid with the above boundary conditions does not result in a loss of accuracy, as compared to a staggered grid without pressure boundary conditions. Upon discretization, the system of linear equations can be written in matrix form as a generalized complex eigenvalue system,

$$\boldsymbol{L}\boldsymbol{x} = \mathrm{i}c\boldsymbol{Q}\boldsymbol{x}, \tag{3.3}$$

where the vector $\boldsymbol{x}$ contains the real and imaginary parts of small perturbations,

$$\boldsymbol{x} = (V_r, V_\theta, V_z, P, X, \Psi)^{\mathrm{T}}, \tag{3.4}$$

and $\boldsymbol{L}$ and $\boldsymbol{Q}$ are constant matrices, which depend on the basic shearing flow. The growth rate ($\lambda = -\mathbf{Im}(c)$) of the perturbation amplitude can be written in the explicit functional form

$$\lambda = \lambda(Re_1, Re_2, \eta, \varepsilon, \alpha, \delta, J, M, D_s, k, n). \tag{3.5}$$

It has been known that the flow system is unstable while the growth rate of the most unstable mode is positive. The converse is true for the negative growth rate. In this paper, the resulting algebraic generalized eigenvalue problem (3.3) is solved by using the software package MATLAB based on the QZ algorithm. To filter out spurious eigenmodes, the number of collocation points is increased until genuine modes are clearly identified. The convergence of the numerical method is shown in table 1, where N is the number of collocation points for each fluid region along a radial direction. It shows that $N = 21$, which is adopted in the rest of paper unless specially stated, is sufficient for the computation of linear stability. The accuracy of the numerical

N	$-\mathbf{Im}(c)$	$\mathbf{Re}(c)$
6	0.07690273	−25.62240581
11	0.08230771	−25.62472117
16	0.08230736	−25.62472144
21	0.08230736	−25.62472144
26	0.08230736	−25.62472144

TABLE 1. Eigenvalue corresponds to the most unstable mode for a different number of collocation point, with $k = 1.0$, $n = 1.0$, $\eta = 0.4$, $\varepsilon = 0.7$, $\delta = 1.0$, $\alpha = 2.0$, $J = 10^3$, $M = 1.0$ and $D_s = 0$, whereas $Re_1 = 50.0$ and $Re_2 = -10.0$.

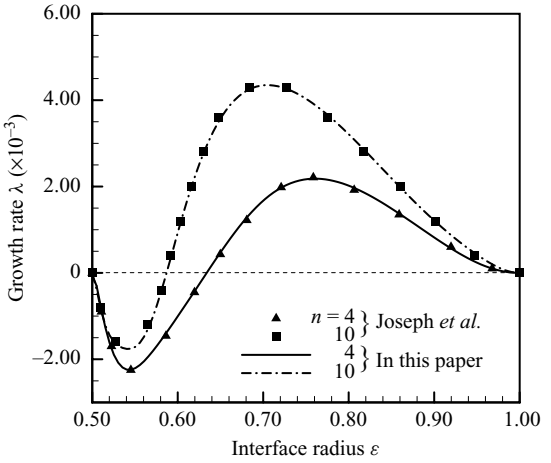

FIGURE 2. Comparison between the results (figure 1) of Renardy & Joseph (1985) and the present work in the absence of a surfactant, with $\eta = 0.5$, $\delta = 1.0$, $\alpha = 0.4$, $J = 0$, $M = 0$, the azimuthal mode $n = 4$, 10 and axial wavenumber $k = 0.1$.

method is verified by comparing the results with those available for Couette flow of two fluids between concentric cylinders without a surfactant (Renardy & Joseph 1985) and confirming excellent agreement (see figure 2).

4. Results and discussion

4.1. *Effect of surface tension on instability*

For completeness, we begin by considering the perturbation flows driven by a perturbed pressure induced by surface tension via a deflection of cylindrical interface in the absence of surfactant and differences of density and viscosity across the interface. The flow instability with stationary outer cylinder is studied first. Figure 3 shows neutral stability curves delineating the boundary between stable and unstable regions in the Re_1 (Reynolds number)–k (wavenumber) plane with parameters $Re_2 = 0.0$, $\eta = 0.4$, $\varepsilon = 0.6$, $\delta = 1.0$, $\alpha = 1.0$ and $M = 0.0$. A neutral condition follows by equating perturbation growth rate λ to zero. The flow contained in the zone with growth rate $\lambda > 0$ is unstable, whereas the converse is true in the zone with $\lambda < 0$. Numbers marked on the curve denote the critical value of azimuthal mode n. The points corresponding to the change in n are distinguished by vertical bars. For $J = 0$,

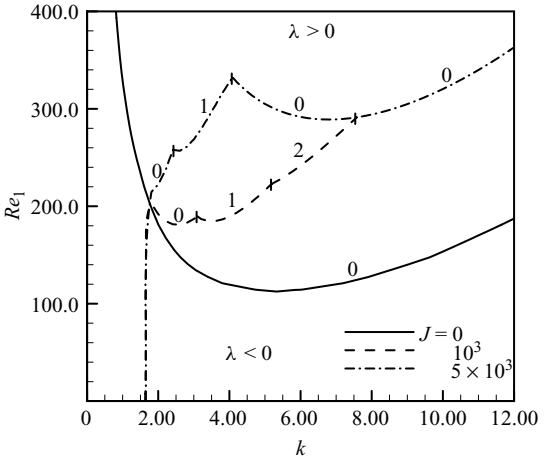

FIGURE 3. Neutral stability curves on the Re_1–k plane with J as a parameter, for $Re_2 = 0.0$, $\eta = 0.4$, $\varepsilon = 0.6$, $\delta = 1.0$, $\alpha = 1.0$, $M = 0.0$ and $D_s = 0.0$.

in the absence of surface tension, flow instability is dominated by the Taylor–Couette instability mechanism shown in the solid line, with an unstable region above the line. The unstable perturbation modes start at critical Reynolds number $Re_1 = 112.5$ at $k = 5.32$ with azimuthal mode $n = 0$. For $J > 0$, however, as noted in § 2.3, surface tension destabilizes the long axisymmetric perturbation waves ($n = 0$, $k < 1/\varepsilon$). The critical axial wavenumber ($k = 1/\varepsilon$), corresponding to the Rayleigh–Tomotika threshold, depends only on the position of the interface. This explains why the neutral curves are nearly coincident for different J ($J > 0$) at a low Reynolds number, where the flow instabilities are dominated by the axisymmetric ($n = 0$) capillary mode. As Re_1 increases further, flow instability is dominated by the interaction of Taylor–Couette and capillary instability mechanisms. The critical azimuthal mode switches from axisymmetric mode ($n = 0$) to non-axisymmetric mode ($n = 1$ or 2). Because the surface tension stabilizes the non-axisymmetric and short-wave modes, the critical azimuthal mode switches to $n = 0$ while the axial wavenumber k is large enough (e.g. $k > 4.10$ for $J = 5 \times 10^3$). The flow instability is dominated by the Taylor–Couette instability mechanism. The neutral curve for $J = 10^3$ tends to be nearly coincident with that for $J = 5 \times 10^3$ as $k > 7.58$. In figure 3, no interval of Reynolds number Re_1, in which the flow is linear stable for all range of k, can be found in the presence of surface tension. The flow is constantly linearly unstable for $J > 0$.

4.2. *Interaction between surface tension and density difference*

In this section, the density difference between fluid 1 and 2 is considered. The flow instability is dominated by the influences of surface tension, density stratification and Reynolds stresses of basic shearing flow. The Yih and Marangoni instabilities due to viscosity stratification and surfactant concentration gradient are ignored with $\alpha = 1.0$ and $M = 0$. From (2.31) in § 2.3, we know the density stratification plays a stabilizing role with the denser fluid coating the outer cylinder. Thus, a stable flow is possible to be achieved with $\delta < 1.0$, even if the surface tension is considered. From § 2.2, we know that the influence of density stratification is introduced through (2.21*a*) corresponding to the balance of normal stress at the interface ($r = \varepsilon$). Combining

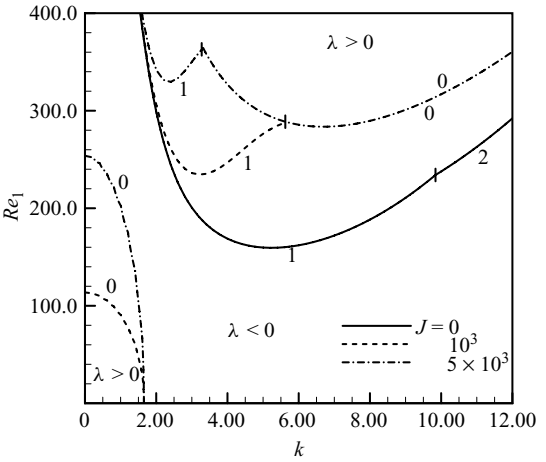

FIGURE 4. Neutral stability curves on the Re_1–k plane with J as a parameter, for $Re_2 = 0.0$, $\eta = 0.4$, $\varepsilon = 0.6$, $\delta = 0.5$, $\alpha = 1.0$, $M = 0.0$ and $D_s = 0.0$.

with $n = 0$, it can be written as

$$[\![2\mathrm{D}V_r - P]\!] + \left[J\frac{1-\varepsilon^2k^2}{\varepsilon^2} - (1-\delta)\frac{\overline{u}_\theta(\varepsilon)^2}{\varepsilon}\right]X = 0, \tag{4.1}$$

where $\overline{u}_\theta(\varepsilon)$ is the shearing velocity of basic flow at the interface. With the second term in (4.1) equalling zero, the influence of surface tension can be counterbalanced by the density stratification with the expression of corresponding interfacial velocity of basic shearing flow $\overline{u}^c_\theta(\varepsilon)$:

$$\overline{u}^c_\theta(\varepsilon) = \sqrt{J\frac{1-\varepsilon^2k^2}{\varepsilon(1-\delta)}}. \tag{4.2}$$

According to (2.9*a*) or (2.9*b*) with $r = \varepsilon$ and $Re_2 = 0$, the corresponding rotation Reynolds number of the inner cylinder can be obtained as

$$Re^c_1 = \sqrt{\frac{J}{1-\delta}\frac{1-\varepsilon^2k^2}{\varepsilon}\frac{\varepsilon}{1-\varepsilon^2}\frac{1-\eta^2}{\eta}}. \tag{4.3}$$

For $k < 1/\varepsilon$, Re^c_1 is available only if $\delta < 1.0$. This indicates that the unstable modes caused by surface tension are possibly stabilized only if the denser fluid coats the outer cylinder. Renardy & Joseph (1985) concluded that it was possible to achieve stability with a denser fluid coating the inner cylinder when the centrifugal effect was overcome by a combination of interfacial surface tension. This conflict is caused by the fact that, according to current research, the contribution of viscosity stratification is ignored by setting $\alpha = 1.0$ (fluids 1 and 2 have the same viscosity). But in Renardy & Joseph (1985), though it was engaged to consider the influence of surface tension and density difference on the flow instability, the effect of viscosity stratification was also included by assuming that the lower viscosity fluid is coating the outer cylinder. Therefore, the stable modes, which are considered to be caused by the interaction of surface tension and density stratification in Renardy & Joseph (1985), are actually attributed to the interaction of surface tension and viscosity stratification.

Figure 4 shows neutral stability curves with $\eta = 0.4$, $\varepsilon = 0.6$, $\delta = 0.5$ and J as a parameter. The axisymmetric unstable modes caused by surface tension are

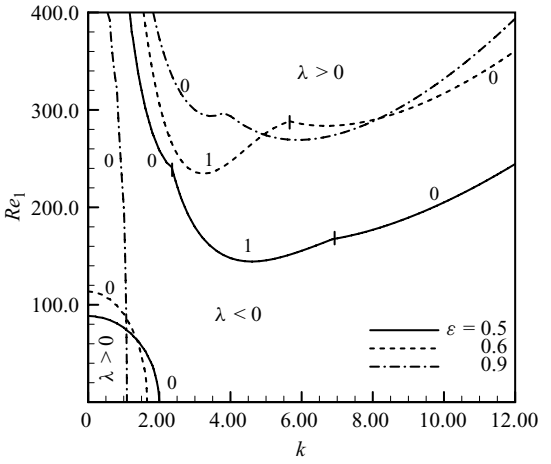

FIGURE 5. Neutral stability curves on the Re_1–k plane with interface position ε as a parameter, for $Re_2 = 0.0$, $\eta = 0.4$, $\delta = 0.5$, $\alpha = 1.0$, $J = 10^3$, $M = 0.0$ and $D_s = 0.0$.

stabilized while the inner cylinder rotates with moderate speed. The unstable domain is separated into two regions, corresponding to a neutral curve with upper and lower branches. The modes constrained in the lower branch are unstable, corresponding to the capillary instability. The profile of the lower branch can be described by (4.3). For $J = 10^3$ and in the limit $k \to 0$, we have $Re_1 = 113.7$ from (4.3), at which the lower branch of the neutral curve joins the vertical axis. On the other hand, the unstable perturbation modes to the upper branch start at the critical Reynolds number $Re_1 = 234.5$ with $k = 3.21$. Thus, as $113.7 < Re_1 < 234.5$, the flow is linearly stable for perturbation with all axial wavenumbers. Figure 5 illustrates the influence of the interface position on the neutral curves. An interval of Reynolds number Re_1 within which the flow is linearly stable for all axial wavenumbers can also be identified (e.g. $88.5 < Re_1 < 144.3$ for $\varepsilon = 0.5$). However, as the interface is closed to the outer cylinder ($\varepsilon \to 1.0$), from (4.3) we know that the critical Reynolds number, at which the capillary instability can be suppressed in the limit $k \to 0$, is $Re_1 \to \infty$. Thus, as demonstrated in figure 5, for example $\varepsilon = 0.9$, no interval of Re_1 for stable flow can be found anymore.

4.3. *Interaction between surface tension and viscosity difference*

Renardy & Joseph (1985) studied the stability of two-fluid Taylor–Couette flow with viscosity stratification and surface tension. The flow with a small Reynolds number was considered. They concluded that a thin layer of the less viscous fluid next to either cylinder is linearly stable in the presence of surface tension. In this section, we shall show that the stable range of interface radii will be extended due to the influence of basic shearing flow. An interval of rotation Reynolds number Re_1, within which the flow is linearly stable, can be identified. Hooper & Boyd (1983) studied the Couette flow of two fluids of different viscosity and found that when viscosity, rather than inertia, is the dominant physical effect, the instability arises at the interface between the two fluids and occurs for short wavelengths. Figure 6(*a*) shows the growth rate of perturbation versus interface position in the absence of surface tension ($J = 0$) with less viscous fluid coating the inner cylinder ($\alpha = 0.5$). For small Reynolds number $Re_1 = 1.0$, the results suggest that the stable range of interface radii is reduced with an increase of azimuthal mode n. This means that the less viscous fluid should be very

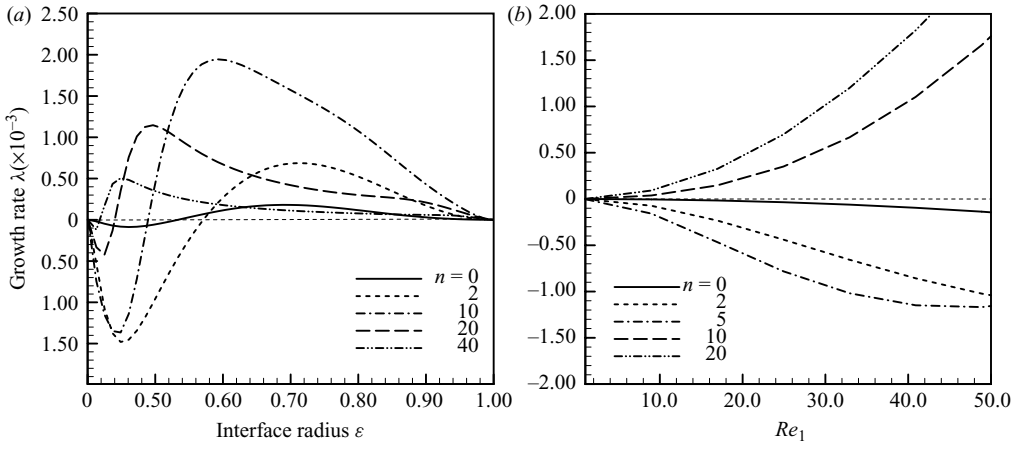

FIGURE 6. Growth rate λ vs. (*a*) interface position ϵ with $Re_1 = 1.0$ and azimuthal wavenumber n as a parameter, (*b*) Reynolds number Re_1 with $\varepsilon = 0.5$ and azimuthal wavenumber n as a parameter. The remaining parameters are $Re_2 = 0.0$, $k = 1.0$, $\eta = 0.4$, $\delta = 1.0$, $\alpha = 0.5$, $J = 0$, $M = 0.0$ and $D_s = 0.0$.

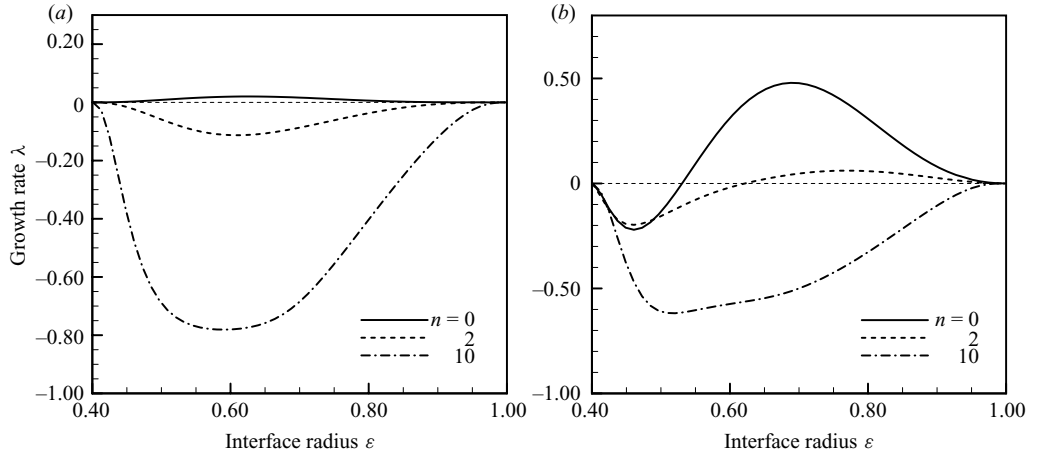

FIGURE 7. Growth rate λ vs. interface position ϵ with azimuthal wave number $n = 0$ (showing λ), $n = 2$ (showing 0.1λ) and $n = 10$ (showing 0.01λ), whereas (*a*) $Re_1 = 1.0$ and (*b*) $Re_1 = 50.0$. The remaining parameters are $Re_2 = 0.0$, $k = 1.0$, $\eta = 0.4$, $\delta = 1.0$, $\alpha = 0.5$, $J = 10$, $M = 0.0$ and $D_s = 0.0$.

thin to keep the flow stable. In figure 6(*b*), the growth rate is plotted against Re_1 in the absence of surface tension with $\alpha = 0.5$ and $k = 1.0$. As Re_1 is raised, growth rates of axisymmetric mode ($n = 0$) are negative and they monotonically decrease. The converse is true for the perturbation with large azimuthal modes (e.g. $n = 10, 20$). This indicates that the viscosity stratification can stabilize the axisymmetric perturbation waves but destabilize the non-axisymmetric perturbation waves with large azimuthal mode n in the presence of basic shearing flow.

Figure 7 shows the influence of rotation Reynolds number Re_1 on the growth rate with $J = 10$. As we expected, for $Re_1 = 1.0$ in figure 7(*a*) the non-axisymmetric mode of perturbation is stabilized, whereas the axisymmetric mode is destabilized due to the effect of surface tension. The flow is constantly unstable wherever the

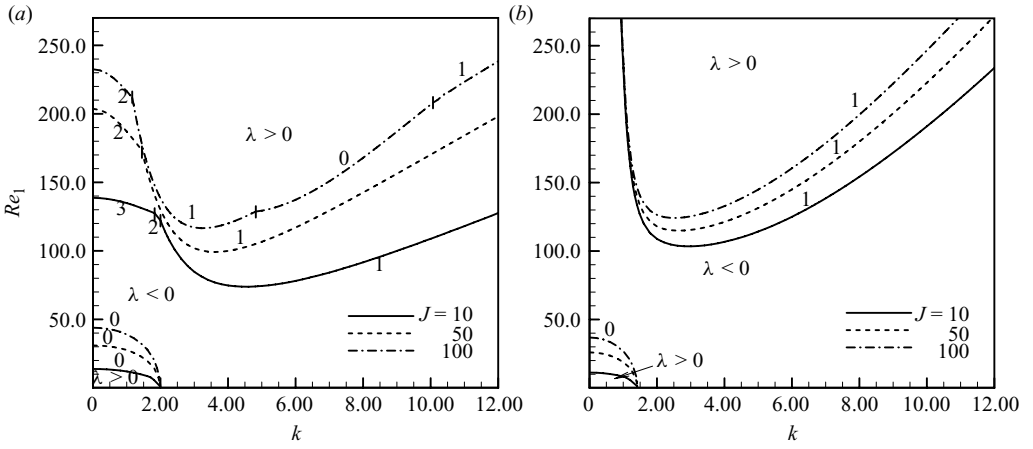

FIGURE 8. Neutral stability curves on the Re_1–k plane with J as a parameter for (a) $\varepsilon = 0.5$ and $\alpha = 0.5$; (b) $\varepsilon = 0.7$ and $\alpha = 2.0$. The remaining parameters are $Re_2 = 0.0$, $\eta = 0.4$, $\delta = 1.0$, $M = 0.0$ and $D_s = 0.0$.

interface locates. However, when Re_1 is raised to 50.0 in figure 7(b), the axisymmetric mode ($n = 0$) displayed is stable while the interface is close to the inner cylinder with $\varepsilon < 0.53$. The stable range of the interface radii is extended with increase of n, which is totally opposite to what is occurring in figure 6(a). This result suggests that the axisymmetric mode of perturbation is stabilized by viscosity stratification in the presence of basic shearing flow, and the non-axisymmetric modes are stabilized by surface tension synchronously. Similar results can also be received with less viscous fluid coating the outer cylinder ($\alpha > 2.0$).

Figure 8 shows neutral stability curves with J as a parameter. Similar to figure 4, the unstable domain is separated into two regions with upper and lower neutral branches. Within the lower branch, flow instability is dominated by the capillary mode ($n = 0$), which can be stabilized with moderate Re_1. As illustrated in figure 8(a), for $J = 10$, $\varepsilon = 0.5$ and $\alpha = 0.5$, shown with a solid line, the corresponding lower branch joins the vertical axis at $Re_1 = 13.8$. The unstable perturbation mode to the upper branch, starting at $Re_1 = 73.8$, corresponds to a non-axisymmetric short wave instability ($n = 1$, $k = 4.61$). Therefore, as $13.8 < Re_1 < 73.8$, the flow is linearly stable for perturbation with all axial wavenumbers. In the limit $k \to 0.0$, the upper branch joins the vertical axis at $Re_1 = 138.7$, corresponding to a non-axisymmetric ($n = 3$) long-wave instability. Physically, this is the consequence of the interaction of capillary instability and Yih instability mechanisms. Similar remarks can be made for $J = 100$, shown in a dash-dotted line. The lower branch joins the vertical axis at $Re_1 = 43.9$, and the unstable mode to the upper branch starts at $Re_1 = 116.5$. The main effect of raising the surface tension is to elevate the neutral curves, thereby expanding the range of stable Reynolds number. In this sense, increasing J has a stabilizing influence. Figure 8(b) illustrates the neutral curves with the less viscous fluid coating the outer cylinder for $\varepsilon = 0.7$ and $\alpha = 2.0$. Similar to figure 8(a), the range of Re_1, in which the flow is stable, can also be identified.

4.4. *Marangoni effect on flow instability*

In general, the presence of even minute amounts of surfactant on a fluid–fluid interface can have a substantial effect on the evolution of the interface (Edwards *et al.* 1991). In

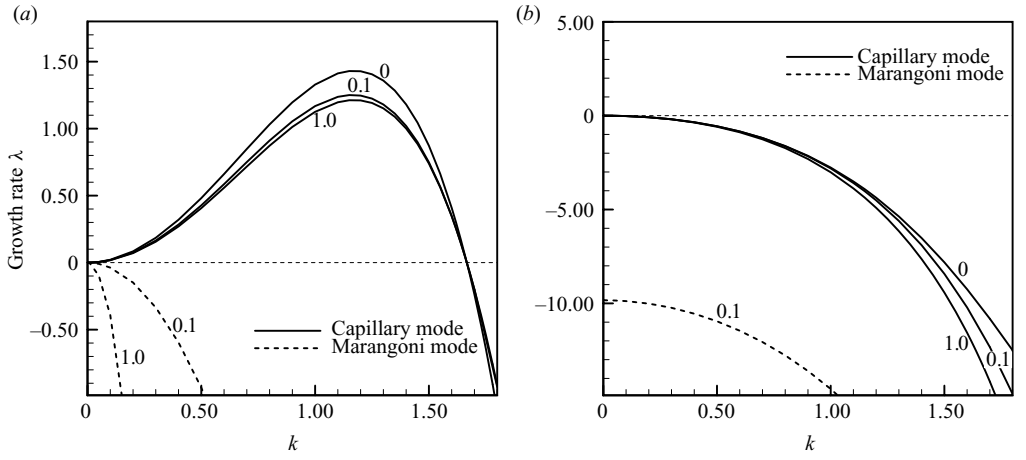

FIGURE 9. Growth rate λ of capillary and Marangoni modes vs. axial wavenumber k at quiescent basic state ($Re_1 = Re_2 = 0$) with Marangoni number M as a parameter, for (a) axisymmetric perturbation $n = 0$ and (b) non-axisymmetric perturbation $n = 1$, and for $\eta = 0.4$, $\varepsilon = 0.6$, $\delta = 1.0$, $\alpha = 1.0$, $J = 10^3$ and $D_s = 0.0$.

this section, we discuss the influence of surfactant on the flow instability characteristics. The influences of density and viscosity stratification are ignored first by setting $\alpha = 1.0$, $\delta = 1.0$. For the quiescent basic state, the flow instability is controlled by the capillary and Marangoni instability mechanisms. Two most important modes can be identified. As illustrated in figure 9(a), the first mode (referred to as the capillary mode), which is unstable for the axisymmetric long perturbation waves, dominates the flow instability. The growth rate of the capillary mode is reduced with an increase of Marangoni number M. This physically indicates that the flow instability is relieved as surfactant is introduced (Otis *et al.* 1993; Cassidy *et al.* 1999; Kwak & Pozrikidis 2001). The second mode, referred to as Marangoni mode, is constantly stable with a negative growth rate. In figure 9(b), for non-axisymmetric perturbations ($n = 1$), the growth rates of both capillary and Marangoni modes are negative. Thus, for quiescent basic state, the surfactant is responsible for introducing a stable mode and the flow instability is still dominated by capillary modes. This can also be demonstrated from an energy viewpoint. In § 2.3, I_3 is the energy supplied corresponding to the surfactant. For quiescent basic state ($Re_1 = Re_2 = 0$), we know that I_3 is always negative. Thus, the surfactant plays a role in relieving the flow instability.

Figure 10 illustrates the effect of basic shearing flow on the growth rate of perturbation with $k = 1.0$, $\varepsilon = 0.6$ and $J = 10^3$. Results are shown both for clean ($M = 0.0$) and contaminated ($M = 0.1$ and $M = 1.0$) interfaces. At a non-zero Reynolds number, an infinite number of normal modes arise. The dominant capillary and Marangoni modes can be identified by parameter continuation with respect to the Reynolds number. In figure 10(a), for axisymmetric ($n = 0$) perturbations, the growth rates of capillary modes are positive over the range of Reynolds numbers considered, whereas the growth rates of Marangoni modes are negative. The basic shearing flow has few effects on the growth rates of perturbations. This behaviour is also entirely consistent with the energy analysis in § 2.3. For $n = 0$, I_3 is always negative and independent of the basic shearing flow. In figure 10(b), for non-axisymmetric ($n = 1$) perturbations with $k = 1.0$, the growth rates of capillary modes are negative, and for the contaminated interface (e.g. $M = 0.1$), they rapidly decrease towards negative

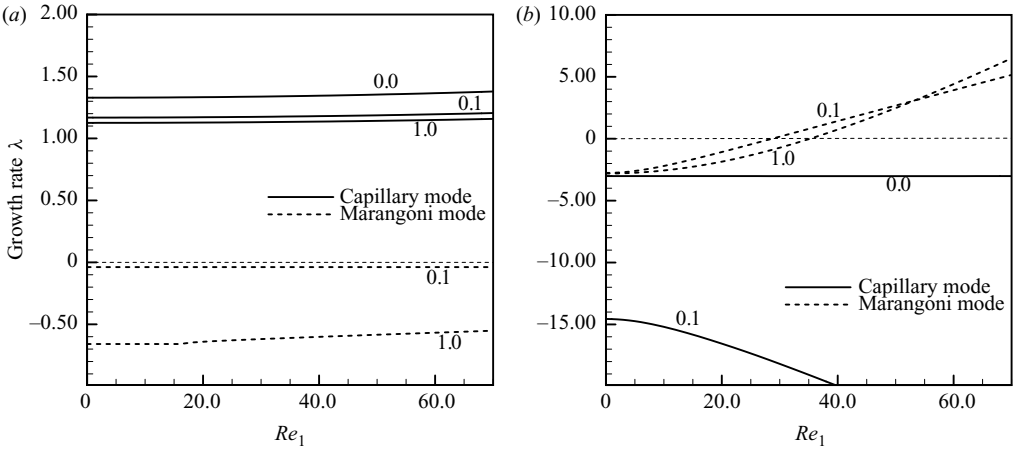

FIGURE 10. Effect of the Reynolds number Re_1 on the growth rate of a wavenumber $k = 1.0$ with Marangoni number M as a parameter, for (a) axisymmetric perturbation $n = 0$ (solid line showing λ and broken line showing 0.01λ) and (b) non-axisymmetric perturbation $n = 1$ (both solid and broken line showing λ), for $\eta = 0.4$, $\varepsilon = 0.6$, $\delta = 1.0$, $\alpha = 1.0$, $J = 10^3$ and $D_s = 0.0$.

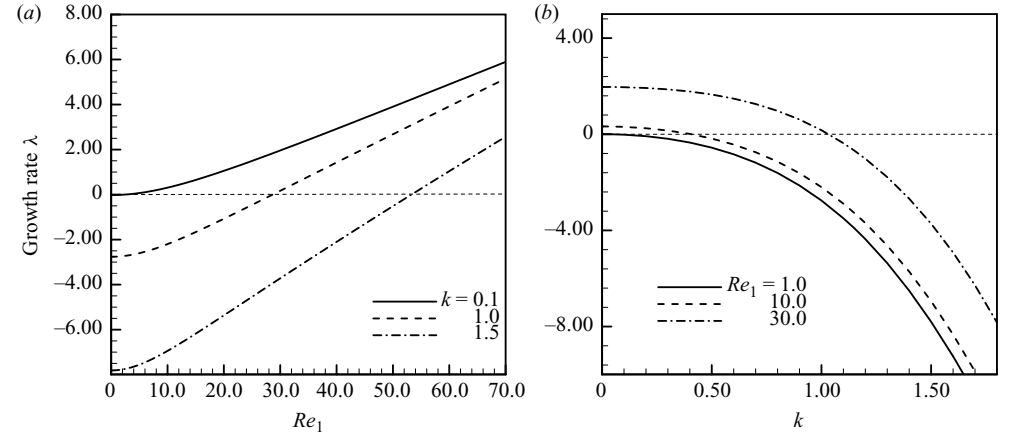

FIGURE 11. Growth rate of non-axisymmetric Marangoni mode ($n = 1$) vs. (a) rotation Reynolds number Re_1 with k as a parameter and (b) axial wavenumber k with Re_1 as a parameter, for $Re_2 = 0.0$, $\eta = 0.4$, $\varepsilon = 0.6$, $\delta = 1.0$, $\alpha = 1.0$, $J = 10^3$ and $D_s = 0.0$.

infinity as Re_1 increases. However, the growth rate of the Marangoni mode is raised monotonically as Re_1 increases. For $M = 0.1$, the corresponding growth rate changes to positive at $Re_1 = 28.7$, and it shifts to $Re_1 = 35.2$ for $M = 1.0$. As Re_1 increases further, the flow instability is then dominated by the Marangoni mode. Similar results are also shown in figure 11(a). For small k, λ changes to positive even if the rotation Reynolds number Re_1 is close to zero (e.g. $\lambda > 0$, whereas $Re_1 > 2.4$ for $k = 0.1$). As illustrated in figure 11(b), the non-axisymmetric Marangoni modes with small k are more unstable than those with large k in the presence of basic shearing flow. Physically, this indicates that the presence of surfactant on the sheared interface

Re_1:	20.0		28.7		38.0	
λ	1.171	−3.808	1.174	−3.812	1.179	−3.816
$\arg(\Psi/V)/\pi$	−0.500	0.500	−0.500	0.500	−0.500	0.500

TABLE 2. Property of the capillary (left-hand columns) and Marangoni (right-hand columns) instability with axisymmetric ($n = 0$) perturbations, for $k = 1.0$, $\eta = 0.4$, $\varepsilon = 0.6$, $\delta = 1.0$, $\alpha = 1.0$, $J = 10^3$, $M = 0.1$ and $D_s = 0.0$, with Re_1 as a parameter.

induces a non-axisymmetric long-wave Marangoni instability, even if it is with small Re_1.

It is interesting to examine in some detail the effect of Marangoni traction force on the flow instability in the presence of basic shearing flow. We know that the Marangoni traction force is induced by the surfactant concentration gradient along the interface. Substituting (2.18) into (2.19) with $D_s = 0.0$, the linearized surfactant convection–diffusion equation, which defines the perturbation of surfactant, can be modified as

$$\left(c + \frac{n}{\varepsilon}\overline{u}_\theta\right)\Psi = -\frac{n}{\varepsilon}V_\theta - kV_z - n\left(\frac{\mathrm{D}\overline{u}_\theta}{\varepsilon} - \frac{\overline{u}_\theta}{\varepsilon^2}\right)X - \frac{1}{\varepsilon}\left(c + \frac{n}{\varepsilon}\overline{u}_\theta\right)X. \tag{4.4}$$

The first two terms on the right-hand side of (4.4) represent the surfactant convection caused by the interfacial perturbation velocity. The third term expresses the correction to the advection of unperturbed surfactant concentration by the change in the basic shearing flow's interfacial velocity, owing to interface displacement. The fourth term corresponds to prescribed surfactant perturbation deriving from the deflection of the cylindrical interface.

For $n = 0$, the third term on right-hand side of (4.4) is zero. The basic shearing flow tends to have little influence. The surfactant concentration is then controlled by the superposition of interfacial perturbation velocity ($V = nV_\theta/\varepsilon + kV_z$, at $r = \varepsilon$) and deflection of cylindrical interface. The capillary mode, which is unstable with $\lambda > 0$ for $k = 1.0$, corresponds to an eigenfunction where the phase shift of surfactant perturbation relative to the interfacial perturbation velocity expressed by $\arg(\Psi/V)/\pi$ is -0.5, as listed in table 2. The sketch of relative wave configuration is shown in figure 12(*a*). The surfactant level is high at crest point A, whereas the converse is true at trough points B and C. The local interfacial perturbation flow is shown with arrows, which drains surfactant from the interface trough and pushes it toward the crest. The resulting surfactant gradient generates Marangoni traction forces that pull the interface back toward the trough, thereby opposing the capillary-induced motion. Thus, the surfactant plays a role in relieving the capillary instability. For the Marangoni mode as listed in table 2, however, the phase shift $\arg(\Psi/V)/\pi$ equals 0.5. The local interfacial perturbation flow direction is totally reversed with surfactant convecting from crest A to trough B, as depicted in figure 12(*b*). The surfactant concentration gradient is then relieved. Therefore, the Marangoni mode is stable with the negative growth rate.

For $n = 1$, according to (4.4), we know that the basic shearing flow has a role in rearranging the surfactant. The concentration gradient is controlled by two competing mechanisms: (i) the basic shearing flow-induced steepening of the surfactant concentration and (ii) local interfacial perturbation flow depletion of the

Re_1:	20.0		28.7		38.0	
λ	−16.552	−1.074	−17.957	0.000	−19.611	1.175
$\arg(\Psi/V)/\pi$	0.486	0.516	0.479	0.502	0.469	0.492
$\lvert\xi\rvert$	0.271	0.908	0.365	0.990	0.461	1.077
$\arg(\xi)/\pi$	−0.369	0.928	−0.335	0.913	−0.305	0.904

TABLE 3. Property of the capillary (left-hand columns) and Marangoni (right-hand columns) instability with non-axisymmetric ($n = 1$) perturbations, for $k = 1.0$, $\eta = 0.4$, $\varepsilon = 0.6$, $\delta = 1.0$, $\alpha = 1.0$, $J = 10^3$, $M = 0.1$ and $D_s = 0.0$, with Re_1 as a parameter.

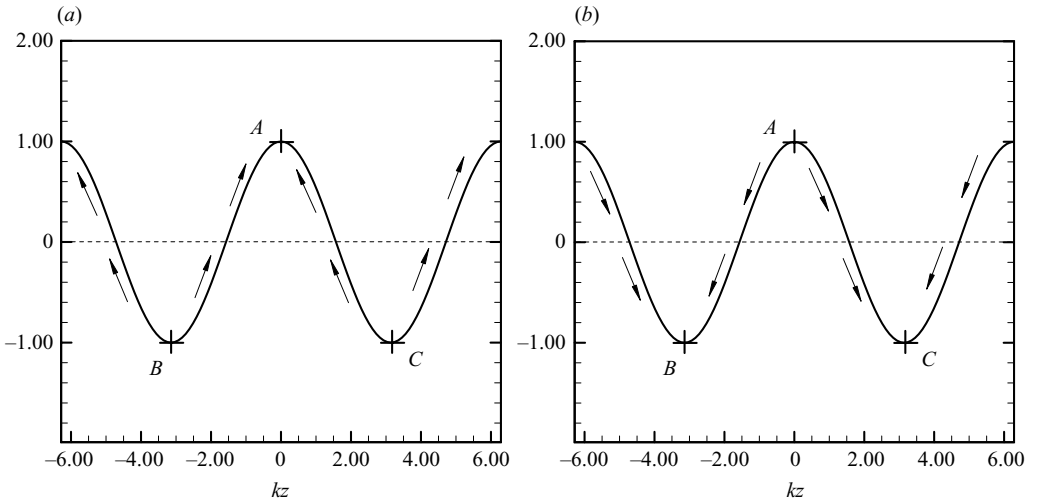

FIGURE 12. Sketch of the Marangoni flows (shown as arrows) of the (*a*) capillary mode and (*b*) Marangoni mode corresponding to table 2.

surfactant concentration. For convenience, we introduce the complex group

$$\xi = \frac{n\,(\mathrm{D}\overline{u}_\theta - \overline{u}_\theta/\varepsilon)}{nV_\theta + \varepsilon k V_z} X, \tag{4.5}$$

which expresses the phase shift and relative amplitude of surfactant concentration perturbations corresponding to the above two effects. In table 3, for capillary mode with the given set of parameters, the phase-shift $\arg(\Psi/V)/\pi$ is close to 0.5 and the relative amplitude expressed by $|\xi|$ is less than 0.5. This denotes that the surfactant concentration is dominated by local interfacial perturbation flow, which convects the surfactant from the region of high concentration to the region of low concentration. The concentration gradient is then relieved and the mode is stable. Similar behaviour can also be observed for the Marangoni mode with small Re_1. The relative amplitude $|\xi|$ is less than 1.0 for the stable mode. However, as Re_1 increases, the relative amplitude $|\xi|$ is raised larger than 1.0. Significant gradient of surfactant concentration is then induced by basic shearing flow, and corresponding Marangoni traction force becomes strong enough to destabilize the flow perturbations. The growth rate of the Marangoni mode is then positive, as listed in table 3. It is worth noting that the perturbation in the basic shearing flow's interfacial velocity due to the displacement of the interface acts to advection surfactant from the crest to the trough, thereby

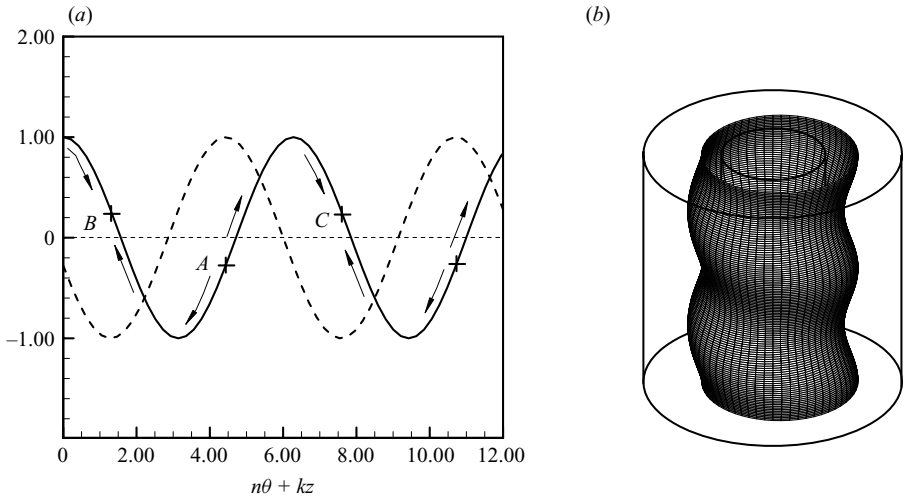

FIGURE 13. Sketch of (*a*) Marangoni flows (shown as arrows) and (*b*) interfacial wave of the Marangoni mode corresponding to table 3.

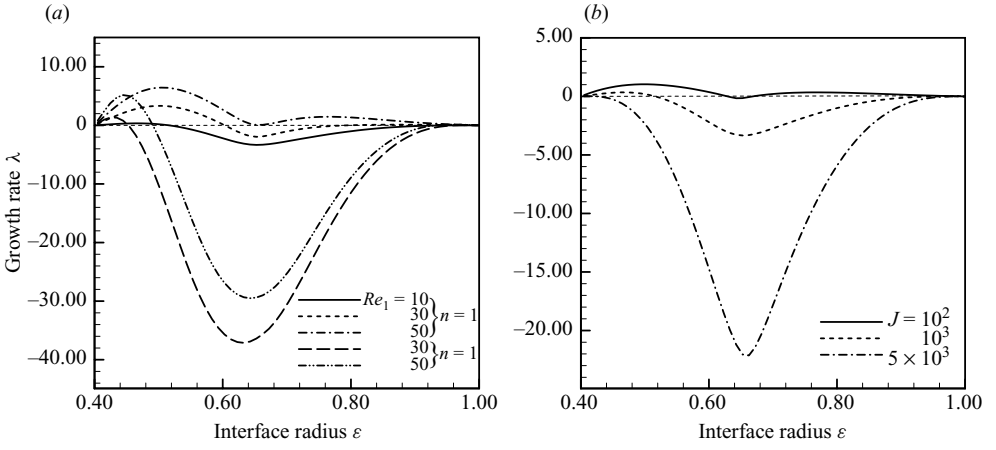

FIGURE 14. Growth rate vs. interface position ε with (*a*) Re_1 as a parameter and $J = 10^3$ and (*b*) J as a parameter and $Re_1 = 10.0$, $n = 1.0$, for $Re_2 = 0.0$, $k = 1.0$, $\eta = 0.4$, $\delta = 1.0$, $\alpha = 1.0$, $M = 0.1$ and $D_s = 0.0$.

introducing a phase-left between the interfacial and surfactant perturbation waves, as illustrated in figure 13(*a*). The interfacial perturbation wave is shown as a solid line and the surfactant perturbation wave is shown as a broken line. The local interfacial perturbation flow is shown as arrows, which tends to relieve the surfactant concentration from high-level point *A* to low-level points *B* and *C*. Figure 13(*b*) illustrates a qualitative approximation of a typical interfacial perturbation wave (corkscrew wave) corresponding to an unstable Marangoni mode. The wave travels in both axial and azimuthal directions.

Figure 14 illustrates the relation between the growth rate of the non-axisymmetric perturbation long wave ($k = 1.0$, $n \neq 0$) and the interface position. In figure 14(*a*), the growth rates are elevated with an increase Re_1. The modes displayed are unstable

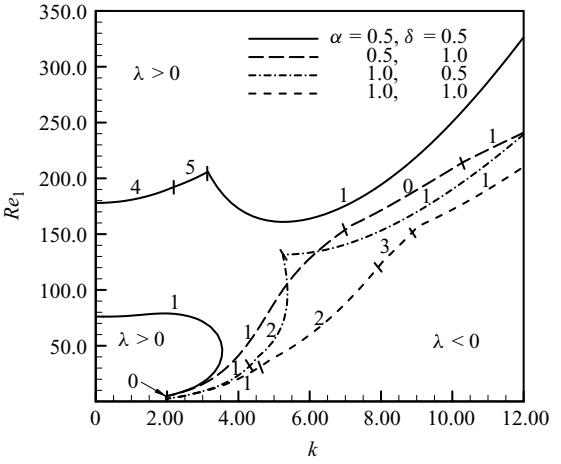

FIGURE 15. Neutral stability curves on the Re_1–k plane with α as a parameter for $Re_2 = 0.0$, $\eta = 0.4$, $\varepsilon = 0.5$, $\delta = 0.5$, $J = 100$, $M = 0.1$ and $D_s = 0.0$.

as ε is close to 0.4. This indicates that the corresponding modes of non-axisymmetric perturbations are more unstable when the interface is close to the inner cylinder. Similar results can also be found in figure 14(*b*), which shows the stabilizing effects of surface tension on the non-axisymmetric perturbations.

In the above case, the influences of viscosity and density stratification are ignored. Note that the non-axisymmetric long perturbation waves are destabilized by Marangoni traction force in the presence of basic shearing flow. In figure 15, for $\alpha = 1.0$ and $\delta = 1.0$, as shown with the short dashed line, the neutral curve begins at $Re_1 = 0$ and $k = 2.0$, corresponding to the capillary mode ($n = 0$), and it switches to the Marangoni mode ($n = 1, 2, 3$) as Re_1 increases. The flow is unstable for the modes on the left upper of the neutral curve. No interval of Re_1 for stable flow can be found and the flow is constantly unstable. Now let us consider the case in the presence of viscosity stratification with denser fluid coating the outer cylinder. From § 4.2 and 4.3, we know that for $\delta < 1.0$, the density stratification plays a stabilizing role in counterbalancing the pressure perturbations induced by surface tension, and the interfacial friction due to viscosity stratification can stabilize the perturbation with small azimuthal mode n in the presence of basic shearing flow. This tends to suggest that the unstable capillary and Marangoni modes can be stabilized at moderate Re_1, as plotted in figure 15 with the solid line. Similar to figure 8(*a*), the unstable domain is separated into two regions. An interval of Re_1 ($78.9 < Re_1 < 161.0$), within which the flow is linearly stable, can evidently be identified. The flow contained within the lower branch corresponds to the instability caused by surface tension and Marangoni traction force. As $k \to 0$, the upper branch starts at $Re_1 = 177.9$ with critical azimuthal mode $n = 4$, which corresponds to the instability induced by interfacial friction.

It is well known that the surfactant diffusion plays a role in homogenizing the concentration distribution. Thus, the Marangoni traction force, which is caused by the gradient of surfactant concentration along the interface, can be relieved with an increase in surfactant diffusivity D_s. Kwak & Pozrikidis (2001) and Luo & Pozrikidis (2006) introduce a dimensionless property group to express the surfactant diffusivity,

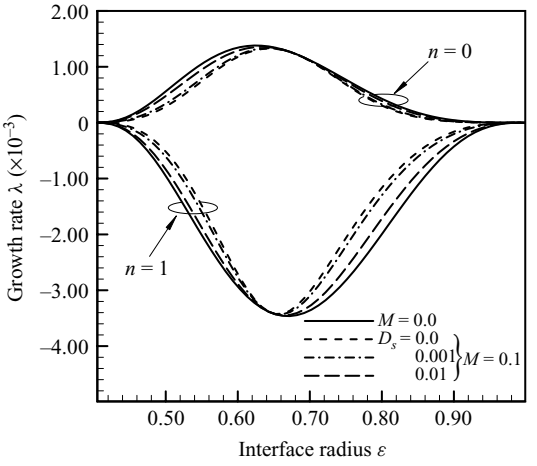

FIGURE 16. Growth rate vs. interface position ε with D_s as a parameter, for $Re_1 = 0.0$, $Re_2 = 0.0$, $k = 1.0$, $\eta = 0.4$, $\delta = 1.0$, $\alpha = 1.0$ and $J = 1.0$.

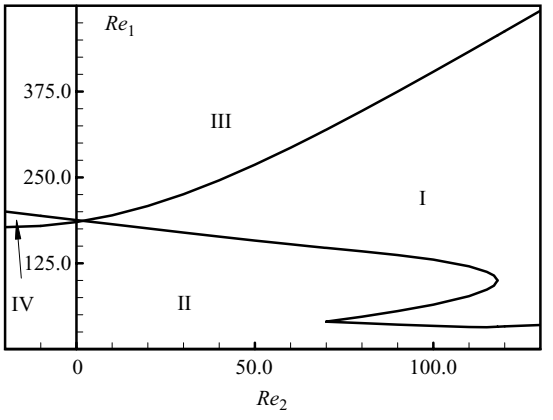

FIGURE 17. Neutral stability curves on the Re_1–Re_2 plane with $J = 500$, $\eta = 0.4$, $\varepsilon = 0.5$, $\delta = 0.5$, $\alpha = 0.5$, $M = 0.1$ and $D_s = 0.001$.

which is defined as

$$\sigma = \frac{\gamma_0^* R_2^*}{\mu^* D_s^*} = \frac{J}{D_s}. \tag{4.6}$$

When σ is small, surfactant diffusion dominates convection, the surfactant concentration is nearly uniform and the motion is similar to that occurring under constant surface tension. Thus, the growth rate is sensitive to the surfactant diffusivity when J is relatively small. As illustrated in figure 16, the growth rate profiles approach the curve with a clean interface ($M = 0$) with an increase in surfactant diffusivity D_s (or a decrease in σ).

4.5. *Rotation of outer cylinder*

In this section, we discuss the influence of the rotation of the outer cylinder on the flow instability. For the single-fluid Taylor–Couette flow, it is well known that the rotation of the outer cylinder has a stabilizing effect on either co-rotation or counter-rotation flow (Sparrow, Munro & Jonsson 1964). However, little attention has been paid to the stratified Taylor–Couette flow. Figure 17 plots the neutral curves on the

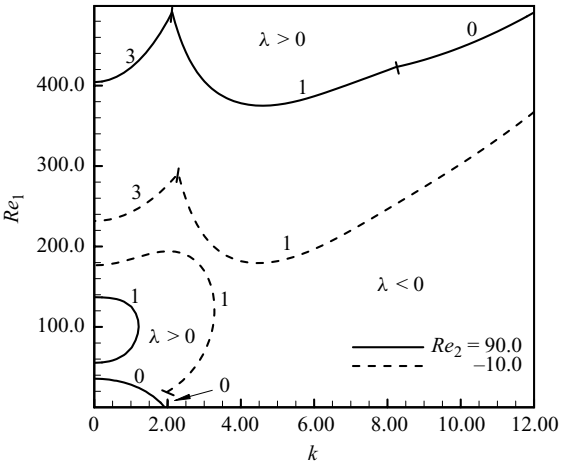

FIGURE 18. Neutral stability curves on the Re_1–k plane, with Re_2 as a parameter, for $\eta = 0.4$, $\varepsilon = 0.5$, $\delta = 0.5$, $\alpha = 0.5$, $J = 500$, $M = 0.1$ and $D_s = 0.001$.

Re_1–Re_2 plane. The influences of density and viscosity stratification, surface tension, Marangoni traction force and Reynolds stress are all considered with parameters $J = 500$, $\eta = 0.4$, $\varepsilon = 0.5$, $\alpha = 0.5$, $\delta = 0.5$, $M = 0.1$ and $D_s = 0.001$. The plane is divided into four zones by two neutral branches. The flow contained within zone I between the upper and lower neutral branches is stable. Zone II is unstable and corresponds to the interfacial instability caused by surface tension and Marangoni traction forces. Zone III is also unstable and denotes the flow instability correlated with viscosity stratification and Reynolds stresses. Zone IV, which demonstrates the overlapped region between zones II and III, is evidently unstable. In § 2.3, the energy supplied due to density stratification (I_1) is proportional to the shearing velocity of basic shearing flow at the interface. Thereby, for $\delta < 1.0$, the stabilizing effects of density stratification are strengthened in the co-rotating state with an increase in Re_2. On the other hand, because energies supplied (I_3, I_4, and I_5) due to viscosity stratification and Marangoni traction force are proportional to the shearing strain of basic shearing flow at the interface, the corresponding destabilizing effects on the flow instability are weakened in the co-rotating state. For this reason, in figure 17, the lower branch of the neutral curve is descended, with Re_2 increasing in the co-rotating state. As $69.9 < Re_2 < 118.0$, a fold of the lower branch can be found. This indicates that there are two stable intervals of Re_1 for a given Re_2. Figure 18 displays the corresponding neutral curve in the Re_1–k plane with $Re_2 = 90.0$. The lower branch is associated with axisymmetric long perturbation waves leading to capillary instability at low Reynolds number $Re_1 < 35.7$. Modes contained within the middle branch with Reynolds number $55.4 < Re_1 < 137.0$ correspond to Marangoni instability induced by surfactant concentration gradient. The upper branch represents the Yih ($n = 3$) and Taylor–Couette instability with critical Reynolds number $Re_1 = 375.0$. Apparently, there are two intervals, $35.7 < Re_1 < 55.4$ and $137.0 < Re_1 < 375.0$, within which the flows are linearly stable for all range of axial wavenumber k. As Re_2 increases, the middle branch shrinks and disappears while $Re_2 = 118.0$. On the contrary, as Re_2 decreases, the middle branch expands and joins the lower branch while $Re_2 = 69.9$.

Another interesting phenomenon worthy to be addressed in figure 17 is zone IV, which demonstrates the overlapped region of zones II and III, while $Re_2 < 1.8$. The neutral curve with $Re_2 = -10.0$ is shown in figure 18, with the two disjointed dashed

lines. As noted above, for the counter-rotation situation, the stabilizing effect of density stratification is weakened while the destabilizing effects of viscosity stratification and Marangoni traction force are strengthened simultaneously. The critical Reynolds number of the lower branch corresponding to stabilize the interfacial instability increases to $Re_1 = 194.0$. The critical Reynolds number of the upper branch starts at $Re_1 = 179.4$. Thus, no interval of Re_1 for stable flow can be found anymore. The flow contained in zone IV is then controlled by the superposition of Marangoni and Taylor–Couette instability mechanisms.

5. Conclusions

This investigation addresses the temporal stability of a pair of radially stratified immiscible liquids in the annular gap between two concentric cylinders rotating independently. The interface is occupied by an insoluble surfactant. The stability determining factors, such as density and viscosity stratification, surface tension, surfactant concentration and Taylor–Couette shearing stress, are all considered and investigated by a comprehensive normal-mode linear instability analysis. The energy analysis is complemented, and a set of energy evolution equations that govern the flow stability is derived to identify the mechanism driving instability. The interaction of these instability mechanisms is discussed. The code has been validated by a successful comparison with the results of previous work without surfactant (Renardy & Joseph 1985).

For all cases with a stationary outer cylinder, at a low rotation Reynolds number of the inner cylinder, instability due to surface tension referred as capillary instability is dominant with destabilizing axisymmetric ($n = 0$) perturbation long waves. The density stratification without gravity plays a stabilizing role if the denser fluid coats the outer cylinder ($\delta = \rho_1/\rho_2 < 1.0$). This stabilizing effect is proportional to the shearing velocity ($\overline{u}_\theta$) of basic shearing flow at the interface. A stable interval of Reynolds number Re_1, within which the capillary instability is stabilized due to density stratification, can be identified. The viscosity stratification, which introduces interfacial friction instability with the presence of basic shearing flow, is associated with instability of the non-axisymmetric large azimuthal mode, whereas stabilizing the axisymmetric mode simultaneously. Hence, an interval of Reynolds number Re_1 within which the flow is stable due to the interaction of capillary and interfacial friction instability can also be determined.

In the presence of a surfactant, Marangoni traction force is induced due to the gradient of surfactant concentration along the interface. For quiescent basic state, Marangoni traction force slows down the effects of surface tension, both for perturbations with axial long wave that they usually destabilize and for those with axial short wave that they usually stabilize. At non-zero Reynolds number, the basic shearing flow can rearrange the surfactant distribution and induce Marangoni traction force to trigger the growth of modes associating with non-axisymmetric ($n \neq 0$) axial long perturbation wave, referred as Marangoni modes. The onset of Marangoni instability can be promoted with the interface surface close to the inner cylinder. The stable interval of the Reynolds number can also be identified when considering the density and viscosity stratification, which play a role in restraining the capillary and Marangoni instability.

Remarkable differences have to be pointed out between the co-rotation and counter-rotation zones. For denser fluid coating the outer cylinder with viscosity stratification, counter-rotation configurations exhibit a destabilizing role in regard to flow instability

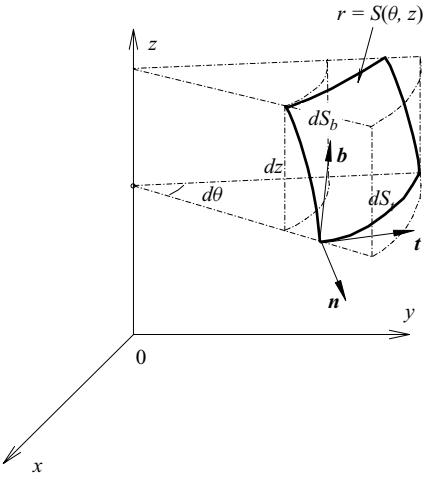

FIGURE 19. Sketch of the surfactant interface.

associating with the non-axisymmetric wave leading to Yih and Marangoni instability mechanisms. The situation is reversed in the co-rotation zone, where the co-rotation of the outer cylinder plays a role in improving the flow stability.

The final manuscript benefits from comments and suggestions provided by three referees. In particular, we are indebted to a referee whose comments and questions have enriched the contents of the paper. This work was supported in part by NSFC under grants 10772097 and 10972115.

Appendix A. Surfactant convection–diffusion equation

The position of the surfactant interface can be defined with surface function $r = S(\theta, z)$, and the surface surfactant concentration is $\Gamma = \Gamma(\theta, z)$ in the cylindrical coordinates. Considering the change of the amount of surfactant ΔN_t from time t to $t+\Delta t$ contained in the control volume ΔV with boundaries $r \in [0, \infty)$, $\theta \in [\theta, \theta+\mathrm{d}\theta]$ and $z \in [z, z+\mathrm{d}z]$, seen in figure 19. For small Δt, we have

$$\Delta N_t = \Delta t \frac{\partial}{\partial t}(\Gamma \boldsymbol{n} \cdot (\boldsymbol{t} \times \boldsymbol{b})\mathrm{d}S_t \mathrm{d}S_b) + O(\Delta t^2). \tag{A 1}$$

Here, $\boldsymbol{n}$ is the unit vector outward normal to the surfactant surface, which can be written as

$$\boldsymbol{n} = \frac{\boldsymbol{e}_r - \dfrac{\partial S}{S\partial\theta}\boldsymbol{e}_\theta - \dfrac{\partial S}{\partial z}\boldsymbol{e}_z}{\sqrt{1 + \left(\dfrac{\partial S}{S\partial\theta}\right)^2 + \left(\dfrac{\partial S}{\partial z}\right)^2}} = \frac{\boldsymbol{e}_r - S'_\theta \boldsymbol{e}_\theta - S'_z \boldsymbol{e}_z}{\sqrt{1 + S'^2_\theta + S'^2_z}}, \tag{A 2}$$

where $\boldsymbol{t}$ and $\boldsymbol{b}$ are the tangent vectors

$$\boldsymbol{t} = \frac{S'_\theta \boldsymbol{e}_r + \boldsymbol{e}_\theta}{\sqrt{1 + S'^2_\theta}}, \quad \boldsymbol{b} = \frac{S'_z \boldsymbol{e}_r + \boldsymbol{e}_z}{\sqrt{1 + S'^2_z}}. \tag{A 3}$$

Note that $\mathrm{d}S_t$ and $\mathrm{d}S_b$ are the side lengths of the surface element

$$\mathrm{d}S_t = \sqrt{\left(1 + S_\theta^{'2}\right)} S \mathrm{d}\theta, \quad \mathrm{d}S_b = \sqrt{\left(1 + S_z^{'2}\right)} \mathrm{d}z, \tag{A 4}$$

where $S_\theta^{'}$, $S_z^{'}$ are defined as

$$S_\theta^{'} = \frac{\partial S}{S \partial \theta}, \quad S_z^{'} = \frac{\partial S}{\partial z}. \tag{A 5}$$

On the other hand, the flux of surfactant in the azimuthal and axial direction during the period of Δt can be written as

$$\begin{aligned} \Delta N_\theta &= \Delta t \Gamma u_\theta \boldsymbol{n} \cdot (\boldsymbol{t} \times \boldsymbol{b}) \sqrt{\left(1 + S_\theta^{'2}\right)} \mathrm{d}S_b \Big|_{\theta + \mathrm{d}\theta} - \Delta t \ \Gamma u_\theta \boldsymbol{n} \cdot (\boldsymbol{t} \times \boldsymbol{b}) \sqrt{\left(1 + S_\theta^{'2}\right)} \mathrm{d}S_b \Big|_{\theta} \\ &= \Delta t \frac{\partial}{\partial \theta} \left[\Gamma u_\theta \sqrt{\left(1 + S_\theta^{'2}\right)} \boldsymbol{n} \cdot (\boldsymbol{t} \times \boldsymbol{b}) \mathrm{d}S_b \right] \mathrm{d}\theta + O(\Delta\theta^2, \Delta t^2), \end{aligned} \tag{A 6}$$

$$\begin{aligned} \Delta N_z &= \Delta t \Gamma u_z \boldsymbol{n} \cdot (\boldsymbol{t} \times \boldsymbol{b}) \sqrt{\left(1 + S_z^{'2}\right)} \mathrm{d}S_t \Big|_{z + \mathrm{d}z} - \Delta t \ \Gamma u_z \boldsymbol{n} \cdot (\boldsymbol{t} \times \boldsymbol{b}) \sqrt{\left(1 + S_z^{'2}\right)} \mathrm{d}S_t \Big|_{z} \\ &= \Delta t \frac{\partial}{\partial z} \left[\Gamma u_z \sqrt{\left(1 + S_z^{'2}\right)} \boldsymbol{n} \cdot (\boldsymbol{t} \times \boldsymbol{b}) \mathrm{d}S_t \right] \mathrm{d}z + O(\Delta z^2, \Delta t^2). \end{aligned} \tag{A 7}$$

If the diffusion of surfactant is considered, there is a corresponding contribution to the amount of surfactant ($\Delta N_{\theta D}$ and ΔN_{zD}) caused by surfactant diffusion crossing from the boundary of control volume. These amounts are given by

$$\begin{aligned} \Delta N_{\theta D} &= D_s (\boldsymbol{n} \times \boldsymbol{b}) \cdot \nabla_s \Gamma \mathrm{d}S_b|_{\theta + \mathrm{d}\theta} - D_s (\boldsymbol{n} \times \boldsymbol{b}) \cdot \nabla_s \Gamma \mathrm{d}S_b|_{\theta} \\ &= D_s \frac{\partial}{\partial \theta} \left[(\boldsymbol{n} \times \boldsymbol{b}) \cdot \nabla_s \Gamma \sqrt{\left(1 + S_z^{'2}\right)} \mathrm{d}z \right] \mathrm{d}\theta + O(\Delta z^2, \Delta t^2), \end{aligned} \tag{A 8}$$

$$\begin{aligned} \Delta N_{zD} &= D_s (\boldsymbol{n} \times \boldsymbol{t}) \cdot \nabla_s \Gamma \mathrm{d}S_t|_{z + \mathrm{d}z} - D_s (\boldsymbol{n} \times \boldsymbol{t}) \cdot \nabla_s \Gamma \mathrm{d}S_t|_{z} \\ &= D_s \frac{\partial}{\partial z} \left[(\boldsymbol{n} \times \boldsymbol{t}) \cdot \nabla_s \Gamma \sqrt{\left(1 + S_\theta^{'2}\right)} S \mathrm{d}\theta \right] \mathrm{d}z + O(\Delta\theta^2, \Delta t^2), \end{aligned} \tag{A 9}$$

where $\nabla_s \Gamma$ is defined as the gradient of surfactant concentration along the surface. It can be written as

$$\nabla_s \Gamma = \frac{\boldsymbol{t}}{\sqrt{\left(1 + S_\theta^{'2}\right)}} \frac{\partial \Gamma}{S \partial \theta} + \frac{\boldsymbol{b}}{\sqrt{\left(1 + S_z^{'2}\right)}} \frac{\partial \Gamma}{\partial z}. \tag{A 10}$$

According to the conservation of surfactant, we know

$$\Delta N_t + \Delta N_\theta + \Delta N_z = \Delta N_{\theta D} + \Delta N_{zD}. \tag{A 11}$$

Considering the limit $\Delta t \to 0$, $\Delta\theta \to 0$ and $\Delta z \to 0$, the surfactant convection–diffusion equation can be written as

$$\begin{aligned} \frac{\partial}{\partial t} (\Gamma S H) + \frac{\partial}{\partial \theta} (u_\theta \Gamma H) + \frac{\partial}{\partial z} (u_z \Gamma S H) &= D_s \frac{\partial}{\partial \theta} \left(\frac{H}{1 + S_\theta^{'2}} \frac{\partial \Gamma}{S \partial \theta} \right) \\ &\quad + D_s \frac{\partial}{\partial z} \left(\frac{S H}{1 + S_z^{'2}} \frac{\partial \Gamma}{\partial z} \right), \end{aligned} \tag{A 12}$$

where H is defined as

$$H = \sqrt{1 + S_\theta'^{\,2} + S_z'^{\,2}}. \tag{A 13}$$

$D_s = D_s^* \rho_2^* / \mu_2^*$ is the dimensionless diffusivity of the surfactant.

Appendix B. Balance of stress on the surfactant interface

The stress balances at the interface are

$$[\![p\boldsymbol{I} - \boldsymbol{\tau}]\!] \cdot (\boldsymbol{t} \times \boldsymbol{b})\, S\sqrt{1 + S_\theta'^{\,2}}\sqrt{1 + S_z'^{\,2}} = J\frac{\partial\left[\Gamma\,(\boldsymbol{n} \times \boldsymbol{t})\, S\sqrt{1 + S_\theta'^{\,2}}\right]}{\partial z} + J\frac{\partial\left[\Gamma\,(\boldsymbol{b} \times \boldsymbol{n})\sqrt{1 + S_z'^{\,2}}\right]}{\partial \theta}, \tag{B 1}$$

where $[\![\cdot]\!] = (\cdot)_2 - (\cdot)_1$ defines the jump notation and J is the parameter used to describe surface tension. Equation (B 1) denotes the balance of pressure, viscosity stress and surface tension at the surfactant interface, which has three components along the cylindrical coordinate directions:

(i) r direction:

$$\frac{1}{J}([\![p - \tau_{rr}]\!] + S_\theta'[\![\tau_{r\theta}]\!] + S_z'[\![\tau_{zr}]\!]) = -\frac{\Gamma}{S}\left(\frac{1}{\sqrt{1 + S_\theta'^{\,2} + S_z'^{\,2}}}\right) + \frac{\partial}{S\partial\theta}\left(\Gamma\frac{S_\theta'}{\sqrt{1 + S_\theta'^{\,2} + S_z'^{\,2}}}\right) + \frac{\partial}{\partial z}\left(\Gamma\frac{S_z'}{\sqrt{1 + S_\theta'^{\,2} + S_z'^{\,2}}}\right), \tag{B 2}$$

(ii) θ direction:

$$\frac{1}{J}(-[\![\tau_{r\theta}]\!] - S_\theta'[\![p - \tau_{\theta\theta}]\!] + S_z'[\![\tau_{\theta z}]\!]) = \frac{\Gamma}{S}\left(\frac{S_\theta'(1 - S_z'^{\,2})}{\sqrt{1 + S_\theta'^{\,2} + S_z'^{\,2}}}\right) + \frac{\partial}{S\partial\theta}\left(\Gamma\frac{(1 + S_z'^{\,2})}{\sqrt{1 + S_\theta'^{\,2} + S_z'^{\,2}}}\right) - \frac{\partial}{\partial z}\left(\Gamma\frac{S_\theta' S_z'}{\sqrt{1 + S_\theta'^{\,2} + S_z'^{\,2}}}\right), \tag{B 3}$$

(iii) z direction:

$$\frac{1}{J}(-[\![\tau_{zr}]\!] + S_\theta'[\![\tau_{\theta z}]\!] - S_z'[\![p - \tau_{zz}]\!]) = \frac{\Gamma}{S}\left(\frac{S_z'(1 + S_\theta'^{\,2})}{\sqrt{1 + S_\theta'^{\,2} + S_z'^{\,2}}}\right) - \frac{\partial}{S\partial\theta}\left(\Gamma\frac{S_\theta' S_z'}{\sqrt{1 + S_\theta'^{\,2} + S_z'^{\,2}}}\right) + \frac{\partial}{\partial z}\left(\Gamma\frac{(1 + S_\theta'^{\,2})}{\sqrt{1 + S_\theta'^{\,2} + S_z'^{\,2}}}\right). \tag{B 4}$$

Substituting (2.11), (2.16) and (2.17) into the above equations, and linearizing both sides at the location of the unperturbed interface, $r = \varepsilon$, the linearized dynamic conditions on the surfactant interface represented by (2.21*a*)–(2.21*c*) can be obtained.

REFERENCES

Baier, G. & Graham, M. D. 1998 Two-fluid Taylor–Couette flow: experiments and linear theory for immiscible liquids between corotating cylinders. *Phys. Fluids* **10** (12), 3045.

Baier, G. & Graham, M. D. 2000 Two-fluid Taylor–Couette flow with countercurrent axial flow: linear theory for immiscible liquids between corotating cylinders. *Phys. Fluids* **12** (2), 294.

Baier, G., Graham, M. D. & Lightfoot, E. N. 2000 Mass transport in a novel two-fluid Taylor vortex extractor. *AIChE J.* **46**, 2395.

Blyth, M. G., Luo, H. & Pozrikidis, C. 2006 Stability of axisymmetric core-annular flow in the presence of an insoluble surfactant. *J. Fluid Mech.* **548**, 207.

Blyth, M. G. & Pozrikidis, C. 2004*a* Effect of surfactants on the stability of two-layer channel flow. *J. Fluid Mech.* **505**, 59.

Blyth, M. G. & Pozrikidis, C. 2004*b* Effect of inertia on the Marangoni instability of two-layer channel flow. Part II. Normal-mode analysis. *J. Engng Math.* **50**, 329.

Carroll, B. & Lucassen, J. 1974 Effect of surface dynamics on the process of droplet formation from supported and free liquid cylinders. *J. Chem. Soc. Faraday Trans.* **70**, 1228.

Cassidy, K. J., Halpern, D. Ressler, B. G. & Grptberg, J. B. 1999 Surfactant effects in model airway closure experiments. *J. Appl. Physiol.* **87**, 415.

Charru, F. & Hinch, E. J. 2000 Phase diagram of interfacial instabilities in a two-layer Couette flow and mechanism of the long-wave instability. *J. Fluid Mech.* **414**, 195.

Diprima, R. C. & Swinney, H. L. 1981 Instability and transition in flow between concentric rotating cylinders. In *Hydrodynamic Instabilities and the Transition to Turbulence*. Springer.

Edwards, D., Brenner, H. & Wasan, D. 1991 *Interfacial Transport Processes and Rheology*. Butterworth-Heinemann.

Frenkel, A. & Halpern, D. 2002 Stokes-flow instability due to interfacial surfactant. *Phys. Fluids* **14**, L45.

Govindarajan, R. 2004 Effect of miscibility on the linear instability of two-fluid channel flow. *Intl J. Multiphase Flow* **30**, 1177.

Halpern, D. & Frenkel, A. 2003 Destabilization of a creeping flow by interfacial surfactant: linear theory extended to all wavenumbers. *J. Fluid Mech.* **485**, 191.

Halpern, D. & Grotberg, J. B. 1993 Surfactant effects on fluid elastic instabilities of liquid lined flexible tubes: a model of airway closure. *Trans. ASME: J. Biomech. Engng* **115**, 271.

Hooper, A. P. & Boyd, W. C. C. 1983 Shear-flow instability at the interface between two viscous fluids. *J. Fluid Mech.* **128**, 507.

Hu, H. H. & Joseph, D. D. 1989 Lubricated pipeling: stability of core-annular flow. Part 2. *J. Fluid Mech.* **205**, 359.

Joseph, D. D., Nguyen, K. & Beavers, G. S. 1984 Nonuniqueness and stability of the configuration of flow of immiscible fluids with different viscosities. *J. Fluid Mech.* **141**, 319.

Joseph, D. D. & Renardy, Y. Y. 1993 *Fundamentals of Two-Fluid Dynamics. Part I. Mathematical Theory and Applications*. Springer.

Joseph, D. D., Renardy, Y., Renardy, M. & Nguyen, K. 1985 Stability of rigid motions and rollers in bicomponent flows of immiscible liquids. *J. Fluid Mech.* **153**, 151.

Khorrami, M. R. 1991 A Chebyshev spectral collocation method using a staggered grid for the stability of cylinder flows. *Intl J. Numer. Meth. Fluids* **12**, 825.

Kull, H. J. 1991 Theory of the Rayleigh–Taylor instability. *Phys. Rep.* **206** (5), 197.

Kwak, S. & Pozrikidis, C. 2001 Effect of surfactants on the instability of a liquid thread or annular layer. Part I. Quiescent fluids. *Intl J. Multiphase Flow* **27**, 1.

Li, X. & Pozrikidis, C. 1997 The effect of surfactants on drop deformation and on the rheology of dilute emulsions in Stokes flow. *J. Fluid Mech.* **341**, 165.

Luo, H. & Pozrikidis, C. 2006 Shear-driven and channel flow of a liquid film over a corrugated or indented wall. *J. Fluid Mech.* **556**, 167.

Newhouse, L. A. & Pozrikidis, C. 1992 The capillary instability of annular layers and liquid threads. *J. Fluid Mech.* **242**, 193.

Otis, D. R., Johnson, M., Pedley, T. J. & Kamm, R. D. 1993 Role of pulmonary surfactant in airway closure: a computational study. *J. Appl. Physiol.* **75**, 1323.

Renardy, Y. & Joseph, D. D. 1985 Couette flow of two fluids between concentric cylinders. *J. Fluid Mech.* **150**, 381.

Schneyer, G. P. & Berger, S. A. 1971 Linear stability of the dissipative, two-fluid, cylindrical Couette problem. Part I. The stably stratified hydrodynamic problem. *J. Fluid Mech.* **45**, 91.

Sharp, D. H. 1984 An overview of Rayleigh–Taylor instability. *Physica* D **12**, 3.

Sparrow, E. M., Munro, W. D. & Jonsson, V. K. 1964 Instability of the flow between rotating cylinders: the wide-gap problem. *J. Fluid Mech.* **20**, 35.

Taylor, G. I. 1923 Stability of a viscous liquid contained between two rotating cylinders. *Phil. Trans. R. Soc. Lond.* A **223**, 289.

Vedantam, S., Joshi, J. B. & Koganti, S. B. 2006 Three-dimensional CFD simulation of stratified two-fluid Taylor–Couette flow. *Can. J. Chem. Engng* **48** (3), 279.

Wei, H. H. 2005 On the flow-induced Marangoni instability due to the presence of surfactant. *J. Fluid Mech.* **544**, 173.

Wei, H. H. & Rumschitzki, D. S. 2005 The effects of insoluble surfactants on the linear stability of a core-annular flow. *J. Fluid Mech.* **541**, 115.

Yarin, A. L., Gelfgat, A. Yu & Bar-Yoseph, P. Z. 2002 Enhancement of mass transfer in a two-layer Taylor–Couette apparatus with axial flow. *Intl J. Heat Mass Transfer*. **45**, 555.

Yih, C. S. 1967 Instability due to viscosity stratification. *J. Fluid Mech.* **27**, 337.